

Can *Gaia* find planets around white dwarfs?

Hannah Sanderson^{1,2*}, Amy Bonsor², Alexander Mustill³

¹*Department of Earth Sciences, South Parks Road, Oxford, OX1 3AN, UK*

²*Institute of Astronomy, University of Cambridge, Madingley Road, Cambridge, CB3 0HA, UK*

³*Lund Observatory, Dept. of Astronomy and Theoretical Physics, Lund University, Box 43, 22100 Lund, Sweden*

Accepted XXX. Received YYY; in original form ZZZ

ABSTRACT

The *Gaia* spacecraft presents an unprecedented opportunity to reveal the population of long period ($a > 1$ au) exoplanets orbiting stars across the H-R diagram, including white dwarfs. White dwarf planetary systems have played an important role in the study of planetary compositions, from their unique ability to provide bulk elemental abundances of planetary material in their atmospheres. Yet, very little is known about the population of planets around white dwarfs. This paper predicts the population of planets that *Gaia* will detect around white dwarfs, evolved from known planets orbiting main-sequence stars. We predict that *Gaia* will detect 6 ± 1 planets around white dwarfs: $8 \pm 3\%$ will lie inside 3 au and $30 \pm 10\%$ will be less massive than Jupiter. As surviving planets likely become dynamically detached from their outer systems, those white dwarfs with *Gaia* detected planets may not have planetary material in their atmospheres. Comparison between the predicted planet population and that found by *Gaia* will reveal the importance of dynamical instabilities and scattering of planets after the main-sequence, as well as whether photoevaporation removes the envelopes of gas giants during their giant branch evolution.

Key words: white dwarfs; astrometry; planets and satellites: detection

1 INTRODUCTION

The *Gaia* space satellite has provided an unprecedented level of information on over 1 billion stars in the Milky Way (and beyond) leading to advances across astrophysics from structure and evolution of the Milky Way to tests of General Relativity (Gaia Collaboration et al. 2016, 2018; Collaboration et al. 2020). In providing precision astrometry for all nearby stars, *Gaia* will uncover many companions to those stars, including exoplanets. Uniquely this detection method will access stars at all stages of stellar evolution, including white dwarfs.

Understanding the planetary systems around white dwarfs is key, because these stars potentially reveal planetary composition. Polluted white dwarfs, white dwarfs with metal lines in their spectra, trace the composition of tidally disrupted planetesimals that have been accreted onto the star (Jura & Young 2014). This can provide an opportunity to study the interiors of rocky exoplanets (Harrison et al. 2018; Swan et al. 2021; Zuckerman et al. 2011) and the architecture of planetary systems post-main sequence (Mustill et al. 2018; Veras et al. 2011). Although polluted white dwarfs provide signatures of tidally disrupted bodies, little is known about planets orbiting white dwarfs. Despite, extensive transit and direct imaging surveys (Fulton et al. 2014; Hogan et al. 2011; Faedi et al. 2011; Burleigh et al. 2002; Gould & Kilic 2008; Debes et al. 2005; Xu et al. 2015) only four white dwarf planet can-

didates have been discovered (Sigurdsson et al. 2003; Luhman et al. 2011; Vanderburg et al. 2020; Blackman et al. 2021). One candidate has a semi-major axis around 3 au (Blackman et al. 2021), but the other three planet candidates are in extreme environments: very close (orbital period ~ 1 day) (Vanderburg et al. 2020) or very far (~ 2500 au) (Luhman et al. 2011) from their host star or circumbinary around a white dwarf and pulsar (Sigurdsson et al. 2003). Detailed observations of planets around white dwarfs are lacking.

Most known planets orbit host stars that end their lives as white dwarfs, and models suggest that outer planets should survive post-main sequence stellar evolution (Veras 2016; Mustill & Villaver 2012). The final position of a planet after post-main sequence stellar evolution is determined by the competing effects of mass loss, which moves planets outwards, and tidal forces, which move them inwards. Tidal forces are most significant for massive planets on the AGB, when stars have more extended envelopes (up to several au Mustill & Villaver 2012). Close-in planets may be engulfed, whilst the high luminosity of the AGB star can cause heating and mass loss from the exoplanet atmosphere (photoevaporation Veras 2016; Barker 2020; Bear & Soker 2011). In multi-planet systems, these effects are complicated by the influence of planets on each other and resulting instabilities can lead to ejection of planets or star-planet collisions (Veras et al. 2013).

Although the broad effects are known, detailed modelling of post-main sequence planetary evolution is difficult due to uncertainties in stellar evolution models for the RGB and AGB (e.g. Bertolami 2018; Matthews & Claussen 2018), dif-

* E-mail: hannah.sanderson@exeter.ox.ac.uk

ferent approaches to modelling tidal interactions (Ogilvie 2014), problems quantifying energy sources that contribute to planet common envelope evolution (Ivanova et al. 2013), chaotic evolution of multi-planet systems e.g. Veras et al. (2013) and the uncertainty in the main-sequence population of wide-orbit planets around WD progenitors. Observationally probing the population of planets around white dwarfs would provide us with direct evidence of planets that have survived this post-main sequence evolution, which is vital for improving models of this process.

With its high precision astrometry, *Gaia* presents an unprecedented opportunity to uncover the population of planets orbiting white dwarfs. Crucially, *Gaia* will bridge the gap between the small (< 1 au) semi-major axes of transit surveys and the large (> 10 au) semi-major axes of direct imaging surveys. *Gaia* is predicted to find tens of thousands of planets beyond 1 au (Casertano et al. 2008; Perryman et al. 2014; Ranalli et al. 2018), including some around white dwarfs. Silvotti et al. (2011) show that *Gaia* will uncover planets with masses greater than $2M_J$ around the brightest white dwarfs. Although the epoch photometry has yet yet been released, comparison between HIPPARCOS and *Gaia* proper motion anomalies has already hinted at binarity in two white dwarf systems (LAWD 37, GD 140) Kervella et al. (2019, 2022).

This paper aims to provide a benchmark with which to assess those planets detected around white dwarfs by *Gaia*. The aim is to make predictions for the population of planets that *Gaia* will detect around white dwarfs by evolving the population of planets seen around main-sequence stars. Comparison of these predictions with the population of planets that *Gaia* detects will probe the importance of additional processes, such as dynamical scattering, survival of common envelope evolution or second generation planet formation. If planets are to arrive in the habitable zone around white dwarfs at around 0.01 au, a potential avenue for the origin of life, such processes are key (Agol 2011; Loeb & Maoz 2013; Kaltenegger et al. 2020). This paper starts by predicting the mass and semi-major axes of planets that *Gaia* can detect (§2.1 §3.1). Predictions are then made for the fate of currently detected planets around main-sequence stars (§2.2), which are used to obtain a prediction for the distribution of planets in the *Gaia* detection region that have evolved from the main-sequence via tides and stellar mass loss (§3.2). By combining the *Gaia* detection probabilities and predicted white dwarf planet distribution with the eDR3 white dwarf catalogue (Gentile Fusillo et al. 2021) as described in §2.3 and §3.3, predictions are made for the number of planet detections around white dwarfs with *Gaia*. The implications of these predictions and how they can be used in the future in combination with *Gaia* planet detections is outlined in §4, alongside a discussion of their validity. Finally, we conclude in §5.

2 METHODS

The aim is to predict the population of planets around white dwarfs, as seen by *Gaia*, that evolve from the population of planets seen around main-sequence stars. We consider the fundamental dynamical effects on the orbit of stellar mass loss and tides. Further complications are discussed in §4 and comparison between the predictions in this paper and *Gaia*

detections will determine the importance of these additional processes, including photoevaporation and dynamical scattering.

In order to predict the number of planets *Gaia* will find around white dwarfs that evolved from the main-sequence by tides and mass loss, we consider three main steps:

- (i) Calculation of *Gaia* detection probability as a function of planet mass and semi-major axis.
- (ii) Prediction of a post-main sequence planet distribution as a function of mass and semi-major axis.
- (iii) Convolution of the detection probability and post-main sequence planet distribution as functions of mass and semi-major axis and summation over this convolution to determine how many planets *Gaia* should find around white dwarfs.

The method for each of these steps is described in this section.

2.1 *Gaia* detection probabilities as a function of mass and semi-major axis

In this paper, a signal to noise (S/N) criterion, relating astrometric signal of a planet to the single along scan accuracy per field of view of a *Gaia* measurement, is used to link planet mass and semi-major axis to detection probability. This is the simplest approach to reliably understand which planets have a strong enough signal to be detected by *Gaia* and is commonly used as indicator when comparing different planet detection algorithms (e.g. in Casertano et al. 2008; Ranalli et al. 2018; Perryman et al. 2014). Other subtler signatures, such as RUWE, can also currently be used as an indicator of binarity (Belokurov et al. 2020; Penoyre et al. 2022).

The astrometric signature, α , of a planet is related to the ratio of planet and stellar masses (M_{pl} and M_\star), their separation, a , and the distance to the star, d , as shown in Equation 1.

$$\alpha = \left(\frac{M_{\text{pl}}}{M_\star} \right) \left(\frac{a}{1 \text{ au}} \right) \left(\frac{d}{1 \text{ pc}} \right)^{-1} \quad (1)$$

More massive planets or those further from the star have larger signatures, because they displace the barycentre position further from the centre of the star. The signature is inversely proportional to the distance to the system, because *Gaia* measures angular positions of stars and the angle subtended by the distance between the star and the system's barycentre will decrease with increasing distance to the system. We consider it sufficient to use an average white dwarf mass $M_\star = 0.6M_\odot$ (Hollands et al. 2018) in this work, when calculating α , because the difference in white dwarf masses is small and makes little difference to α in comparison to the large change in astrometric noise with white dwarf magnitude. Additionally, there are several sources of error on the mass values in the catalogue, as discussed in §4.1.4.

Signal can be maximised by looking for planets at large semi-major axes, a . However, the ability of *Gaia* to accurately recover a companion's orbital parameters is limited by mission length. For planets with orbital periods longer than the expected mission length following extensions (ten years), the accuracy of the planet orbital parameters which are recovered decreases (Ranalli et al. 2018). Therefore in this work, a period of ten years has been taken as the cut off for reliable planet detections. This corresponds to $a = 4.64$ au for a

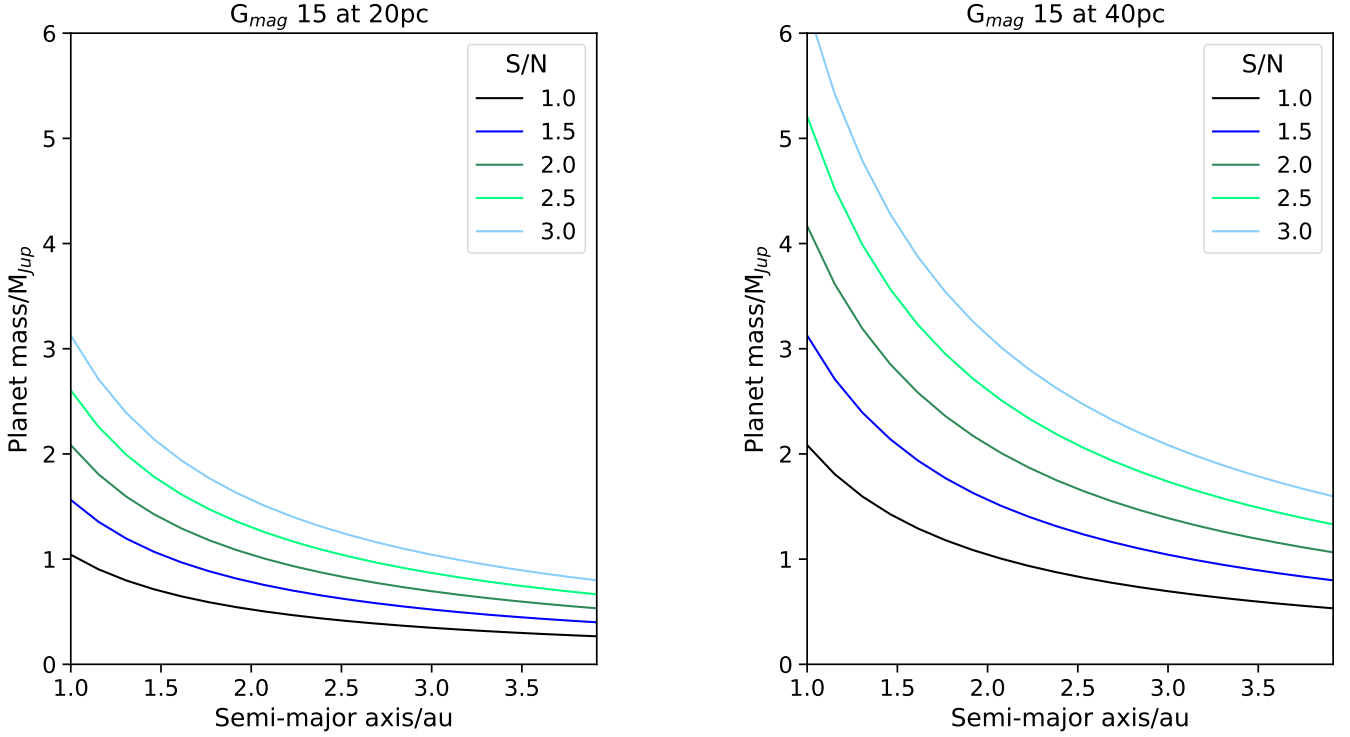


Figure 1. The astrometric signal for a planet with given properties (mass and semi-major axis) compared to the astrometric noise for *Gaia* measurements of a 15th mag white dwarf at 20 pc (left) or 40 pc (right). The semi-major axis range spans positions from the innermost initial position in our simulations to the maximum semi-major axis detectable by *Gaia* due to its ten year mission length (see §2.1). Planets with $S/N > 3$ have an average detection probability of 0.93, whilst planets with $S/N < 1$ have average detection probability of 0.14. Planets less massive than Jupiter will not be detected by *Gaia*.

planet around a $1M_{\odot}$ star or $a = 3.91$ au for a planet around a $0.6M_{\odot}$ white dwarf.

The noise on *Gaia*'s astrometric measurement is the single along-scan accuracy per field of view, σ_{fov} (Perryman et al. 2014). Importantly, σ_{fov} is a function of a star's magnitude. In this work the S/N ratio will be defined as

$$S/N = \frac{\alpha}{\sigma_{\text{fov}}}. \quad (2)$$

Gaia errors for future data releases are publicly available as sky-averaged parallax accuracy σ_{ϖ} not as σ_{fov} . σ_{ϖ} can be converted to σ_{fov} by considering the sky-averaged number of field crossings per star (150 ± 50 for a ten year mission (Ranalli et al. 2018)), the geometrical factor linking the sky-averaged parallax accuracy with the error per field crossing (2.15) and a science contingency margin (1.1 for eDR3 onwards), which covers any additional errors in the modelling process (Perryman et al. 2014).

$$\sigma_{\text{fov}} = \frac{\sqrt{150}\sigma_{\varpi}}{1.1 \times 2.15} \approx 5.18\sigma_{\varpi} \quad (3)$$

This paper uses the predicted errors for Data Release 5, because this data release will have the longest timespan for observations so can detect planets with periods up to ten years. These error estimates are based on *Gaia* eDR3 and are the most up-to-date at the time of press. The errors are described

as:¹

$$\sigma_{\varpi} [\mu\text{as}] = 0.527(40 + 80z + 30z^2)^{\frac{1}{2}}, \quad (4)$$

where z is given by

$$z = \text{MAX}[10^{0.4(13-15)}, 10^{0.4(G-15)}] \quad (5)$$

where G is the broad-band, white-light, *Gaia* magnitude.

S/N can be linked to detection probability. Ranalli et al. (2018) used Markov chain Monte Carlo methods and three information criteria to determine detection probabilities over a grid of S/N and orbital period. Planets with $S/N > 3$ have an average detection probability (across periods less than 10 years) of 0.93, whilst planets with $S/N < 0.7$ cannot be detected. In this work, $p_{ljk}(S/N_{ljk}, P_j)$ denotes the detection probability of a planet with semi-major axis in bin j with period P_j , mass in bin k around white dwarf l and were calculated from the Ranalli et al. (2018) detection probabilities.

2.2 Prediction of the distribution of planets which survive tidal evolution and stellar mass loss to reach the white dwarf phase

The distribution of close-in planets around main-sequence stars is well known from radial velocity and transit observations. Some of these observations, alongside direct imaging surveys, now reach orbital periods of years, as probed

¹ Taken from *Gaia* Mission Science Performance for Data Release 5 <https://www.cosmos.esa.int/web/gaia/science-performance>.

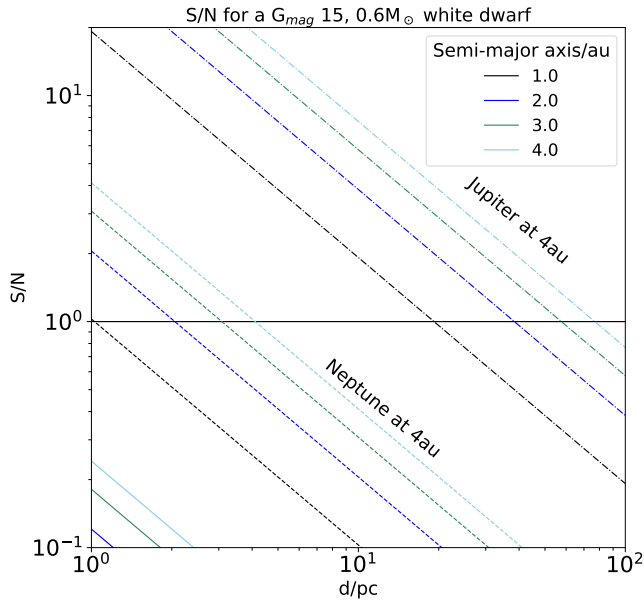


Figure 2. The astrometric signal of a Jupiter or Neptune mass planet on a circular orbit at 1-4 au, compared to the astrometric noise in a *Gaia* measurement for a star at a given distance. The maximum semi-major axis corresponds to the maximum detectable by *Gaia* on a ten year mission observing a $0.6M_{\odot}$, $G_{\text{mag}} = 15$ white dwarf. Dot-dash lines are for a Jupiter mass planet, dash lines are for a Neptune mass planet. A solid horizontal line is for a $S/N = 1$ below which the detection probability drops to zero. Jupiter mass planets are only detectable out to 30 pc. Neptune mass planets are not detectable, because their signal to noise drops below one at 3 pc and there are no white dwarfs within 5 pc (Hollands et al. 2018; Gentile Fusillo et al. 2021).

by *Gaia*, but the planets detected by *Gaia* around main-sequence stars will always provide the most reliable probe of the planetary population of interest on the main-sequence.

Radial velocity (Bryan et al. 2016), transit (Zhu & Dong 2021; Santerne et al. 2016) and direct imaging (Biller et al. 2013) measurements suggest the frequency of giant planets decreases at distances greater than 2-3 au from the star, such that a broken power law is the most appropriate model for the giant planet occurrence rate around main-sequence stars (Fernandes et al. 2019; Fulton et al. 2021). In this work, we use the EPOS, three parameter fit (symmetric) broken power law of Fernandes et al. (2019)².

$$\frac{d^2 N}{d \log P d \log M} = c_0 \left(\frac{P}{P_{\text{break}}} \right)^{p_1} \left(\frac{M}{10 M_{\oplus}} \right)^{m_1} \quad (6)$$

where $c_0 = 0.84 \pm 0.17$, $m_1 = -0.45 \pm 0.05$, $p_{\text{break}} = 1581 \pm 643$ days and

$$p_1 = \begin{cases} 0.65 \pm 0.17 & P < P_{\text{break}} \\ -0.65 \pm 0.17 & P > P_{\text{break}} \end{cases}. \quad (7)$$

This broken power law describes the number of planets per log semi-major axis and log mass bin, $\frac{d^2 N}{d \log P d \log M}$ and models the distribution of planets around main-sequence stars ac-

counting for observation biases. This planet occurrence rate predicts $4.9 \pm 0.7\%$ of stars have planets with masses $1-13 M_J$ with semi-major axes < 20 au. Non-detections are considered by weighting the number of detected planets in a mass and semi-major axis bin by the inverse of the survey completeness. The power law of Fernandes et al. (2019) was used because it reproduced Cumming et al. (2008) earlier results, gave results comparable to direct imaging observations at large semi-major axes and drew on multiple groups of observations (the latest Kepler data release and radial velocity results from Mayor et al. (2011)).

To predict the change in planetary orbits from the main-sequence to the white dwarf phase, the orbital evolution of planets along the AGB was simulated, following the prescription presented in Mustill & Villaver (2012). This model breaks the effects of stellar evolution on planets into three key components: expansion of the planetary system due to mass loss, inward movement of planets due to tidal effects and engulfment of planets which are too close to the star as the star expands. Tidal forces were modelled as viscous dissipation of the equilibrium tide (Zahn 1977). The model calculates the semi-major axis of the orbits of isolated planets and the stellar envelope as a star evolves along the AGB, following the models of Vassiliadis & Wood (1993). Any planet which moves inside the stellar envelope at a given timestep is removed. The limitations of this model are discussed in §4.1.1.

Extending the masses and initial semi-major axes of Mustill & Villaver (2012), we simulated 13,051 planets around a $1M_{\odot}$ progenitor and 12,121 planets around a $1.5M_{\odot}$ progenitor³. The planet masses sampled 31 possible values evenly distributed in log space between Earth and 13 Jupiter masses. Initial semi-major axes ranged from 1 – 10 au. All planets at semi-major axes smaller than this would be engulfed by their host star and those beyond this would be far beyond the *Gaia* detection region so were not considered. Two groups of simulations were carried out. Simulation A was a coarse spacing of 0.03 au to enable sampling of a large range of semi-major axis space. Simulation B and C were a fine spacing of 0.001 au spanning ± 0.12 au ($1 M_{\odot}$) and ± 0.09 au ($1.5 M_{\odot}$) from the initial position of the outermost engulfed planet (determined from Simulation A) at each mass. This fine sampling was to investigate behaviour near the initial semi-major axis of the outermost engulfed planet, because in this region there is large variation in the strength of the tidal forces (see Mustill & Villaver 2012). The parameters for these simulations are summarised in Table 1. The final masses of the white dwarfs (needed for estimating the importance of tidal effects) were $0.5702M_{\odot}$ and $0.6014M_{\odot}$ for the $1M_{\odot}$ and $1.5M_{\odot}$ progenitors respectively.

To combine the main-sequence planet occurrence rate with the results of our simulations, mass and semi-major axis space were split into bins. There were 31 bins equally spaced in $\log M$ from $1M_{\oplus}$ to $13 M_J$ and the semi-major axis bins have variable width corresponding to equispaced period bins from (Ranalli et al. 2018) (average width 0.21 au). This corresponded to the range of initial positions in our simulation.

² The errors in Fernandes et al. (2019) are asymmetric, but this work uses the average of the upper and lower bounds as an estimate of the size of the error.

³ Fewer simulations were needed for the higher mass progenitor because the larger expansion of the planetary system moved most of the sample outside the *Gaia* detection range.

Simulation	Progenitor mass/ M_{\odot}	Spacing/au	Planet mass/ M_J	Semi-major axis range/au
A	1.0, 1.5	0.03	$3.1 \times 10^{-4} - 13$	1-10
B	1.0	0.001	$3.1 \times 10^{-4} - 13$	inner position of outermost engulfed planet ± 0.12
C	1.5	0.001	$3.1 \times 10^{-4} - 13$	inner position of outermost engulfed planet ± 0.09

Table 1. Semi-major axis ranges for simulated planets for each planet mass. 31 planet masses were chosen equally spaced in log space between M_{\oplus} and $13 M_J$. For each planet mass, the above semi-major axes arrays were used for the initial conditions of the simulations. All planets were assumed to be in single planet systems on circular orbits. For discussion of choices of semi-major axis spacing see §2.2.

We assumed the planets were around a $0.6 M_{\odot}$ white dwarf to transform the main-sequence distribution from $\frac{d^2 N}{d \log P d \log M}$ to $\frac{d^2 N}{d \log a d \log M}$ where N is the number of planets per star, a is the semi-major axis, P is the period and M is the planet mass. All logarithms are to base 10 so $d \log a = \frac{da}{a} \log_{10}(e)$ was used to transform from $\frac{d^2 N}{d \log a d \log M}$ to $\frac{d^2 N}{da d \log M}$ where da was the corresponding bin width and a was the midpoint of the bin. In the following equations, the index i represents the initial semi-major axis bin of a planet, j represents the final semi-major axis bin and k represents the mass bin. Planetary mass loss was not modelled so a planet's mass bin does not change during the simulation. All summations are written explicitly.

The predicted occurrence rate of planets around white dwarfs in a given semi-major axis, mass range, $\frac{d^2 N_{WD}}{da d \log M}$ is calculated by

$$\left(\frac{d^2 N_{WD}}{da d \log M} \right)_{jk} = \sum_i R_{ijk} C_{ik}. \quad (8)$$

R_{ijk} is the number of planets of mass labelled by k in the simulation that started in the i^{th} semi-major axis bin, but end the simulations in the j^{th} semi-major axis bin post-main sequence. C_{ik} is the weight of each simulated planet, which is the value of the main-sequence planet distribution from Fernandes et al. (2019) for the centre of the bin, divided by the number of simulated planets initially in the i^{th} bin, B_i .

$$C_{ik} = \left(\frac{d^2 N_{MS}}{da d \log M} \right)_{ik} \frac{1}{B_i} \quad (9)$$

2.3 Predicted numbers of planet detections

2.3.1 Using the eDR3 catalogue

To predict the number of planets *Gaia* will detect around white dwarfs requires the calculation of the parameter space available for planet detection around known white dwarfs. The white dwarf sample, containing mass estimates, *Gaia* broad-band magnitudes (G_{mag}) and parallaxes was obtained from the Gentile Fusillo et al. (2021) catalogue from *Gaia* early Data Release 3, which improved on their previous catalogue from Data Release 2 (Gentile Fusillo et al. 2019). In Gentile Fusillo et al. (2021), each object in the catalogue was assigned a probability of being a white dwarf P_{WD} based on a series of absolute magnitude and colour criteria. In Gentile Fusillo et al. (2021), applying the criteria $P_{WD} > 0.75$ recovered 359,000 high confidence white dwarf candidates with only 1% of contaminant objects. Therefore in this work, we applied three filters to the catalogue to obtain a catalogue of white dwarfs:

- $P_{WD} > 0.75$

- $G_{mag} < 20.7$ - remove objects too faint to be detected by *Gaia*.

- $M < 0.663 M_{\odot}$ - remove white dwarfs with progenitor masses $> 1.5 M_{\odot}$.

After applying these cuts, the sample is reduced to 152,618 white dwarfs out to distances of 13,000 pc.

White dwarfs with high progenitor masses were excluded from the catalogue, because they lose a greater proportion of mass as they evolve off the main-sequence (Cummings et al. 2018) and the surviving planet positions are beyond the maximum semi-major axis detectable by *Gaia* for a ten year mission. This will be discussed further in §3.2 (Figure 5b), where the chosen cut-off is justified based on simulations that indicate that no planets directly evolved from the main-sequence will be detected around stars within initial masses higher than $M_i > 1.5 M_{\odot}$. The final mass cut off was determined using the Cummings et al. (2018) MIST-based initial-final mass relation based on stellar clusters. This gave $M_f = 0.609 \pm 0.054 M_{\odot}$ for a $1.5 M_{\odot}$ progenitor, so an upper limit of $0.663 M_{\odot}$ was adopted.

2.3.2 Combining the predicted planet distribution with Gaia detection probabilities

For each white dwarf in the filtered catalogue, labelled by the index l , the probability of detecting a planet as a function of planet mass, j and planet semi-major axis, k , p_{ljk} was calculated as described in §2.1. The semi-major axis bins were determined from the period bins in Ranalli et al. (2018). The mass bins were unchanged. $\left(\frac{d^2 N_{WD}}{da d \log M} \right)_{jk}$ calculated in §2.2 was recalculated to match these bins for the following calculations.

The distribution of detected planets $\frac{d^2 N_{det}}{da d \log M}$ corresponds to

$$\left(\frac{d^2 N_{det}}{da d \log M} \right)_{jk} = \sum_l p_{ljk} \left(\frac{d^2 N_{WD}}{da d \log M} \right)_{jk}. \quad (10)$$

The number of detected planets is

$$N_{pl} = \sum_{jk} \left(\frac{d^2 N_{det}}{da d \log M} \right)_{jk} (da)_j (d \log M)_k. \quad (11)$$

2.3.3 Error Analysis

The error on the number of planets was calculated by appropriately propagating the errors on each of the quantities in equations 8-11. The error on $\left(\frac{d^2 N_{MS}}{da d \log M} \right)_{ik}$ came from the average of the upper and lower bounds on these values from Fernandes et al. (2019). The error on R_{ijk} (the number of planets of mass labelled by k in the simulation that moved

from the i^{th} to the j^{th} semi-major axis bin in the simulations) was assumed to be Poissonian $\sigma(R_{ijk}) = \sqrt{R_{ijk}}$. The dominant error in the detection probabilities is from the error in the sky-averaged number of field crossings per star (150 ± 50) (Ranalli et al. 2018). The resulting error in the detection probabilities was combined fractionally in quadrature with the error on $\left(\frac{d^2 N_{\text{WD}}}{da d \log M}\right)_{ik}$ to obtain the error on $\left(\frac{d^2 N_{\text{det}}}{da d \log M}\right)_{ik}$. Another possible source of uncertainty is the exclusion white dwarfs with $M > 0.663 M_{\odot}$. This is difficult to quantify so was not included in our error calculations but is discussed in §4.1.4.

3 RESULTS

3.1 What is the probability of *Gaia* detecting a planet as a function of mass and semi-major axis?

Only planets with masses greater than or equal to Jupiter will be detectable by *Gaia* around white dwarfs. The astrometric signal of a planet on a given orbit with a given mass is calculated according to Equation 1 and the noise is calculated by 3. Figure 2 indicates that Neptune mass planets have $S/N > 1$ up to 3 pc and beyond this only Jupiter mass planets have $S/N > 1$. Since the closest white dwarf, 40 Eri B, is at 5.04 pc (Hollands et al. 2018; Gentile Fusillo et al. 2021), this suggests no Neptune mass planets will be discovered around white dwarfs by *Gaia*. As shown in Figure 1, even Jupiter mass planets have a low S/N and correspondingly a low detection probability at small semi-major axes. These calculations were done for a bright white dwarf with $G_{\text{mag}} = 15$. For fainter white dwarfs, the astrometric noise would be larger, decreasing the S/N of a given planet mass and semi-major axis.

Figure 3 shows an example map illustrating detection probability as a function of mass and semi-major axis generated for a $G_{\text{mag}} = 15$ white dwarf. It clearly demonstrates that almost all planets less massive than Jupiter will not be detected by *Gaia*. There is a significant region of parameter space where planets with orbital periods longer than the mission length could be detected, shown by the hashed region in Figure 3, however the recovery of orbital parameters in this region is unreliable. For clarity, planet detections in this region are not included in the predicted number of planets *Gaia* will detect (§3.3).

3.2 What is the planet distribution around white dwarfs?

Predictions for the population of planets surviving to the white dwarf phase are shown in Figure 5a for a $1 M_{\odot}$ progenitor. These should be compared to the initial population of planets on the main-sequence Fernandes et al. (2019) shown in Figure 4 as $\frac{d^2 N_{\text{MS}}}{da d \log M}$. Over the mass and semi-major axis range shown here the main-sequence distribution gives a planet occurrence rate of 0.61 ± 0.01 planets per star. This is to be contrasted with the population surviving to the white dwarf phase, where only 14% of planets initially within 3.91 au (the detection limit due to the length of *Gaia* mission) of $1 M_{\odot}$ progenitor remain. The number of planets per star in

the *Gaia* detection region is lower than the main-sequence, because planets are engulfed or move out of this region as their orbits expand due to stellar mass loss post-main sequence. This is evident from the white regions in Figures 5a where $\frac{d^2 N_{\text{WD}}}{da d \log M}$ is zero. Even fewer planets (0.1%) survive in the detection region around a $1.5 M_{\odot}$ progenitor, because larger mass progenitors have stronger tidal forces and lose a greater proportion of their mass. The majority of the region inside 3.91 au in Figure 5b is white. This means it is very unlikely that planets will be detected around white dwarfs with $M > 1.5 M_{\odot}$ progenitors. This is the basis for the mass cut off applied to the eDR3 catalogue (§2.3), excluding white dwarfs with higher progenitor masses.

Tidal evolution of gas giants leads many planets to migrate inwards: some migrate so far they are engulfed by the stellar envelope. This means that only planets with initial positions sufficiently far out survive to the white dwarf phase. This distance increases with planet mass, as higher mass planets feel a stronger tidal pull from the star. This is demonstrated by the diagonal trend of the boundary between zero and non-zero values of $\frac{d^2 N_{\text{WD}}}{da d \log M}$ in Figures 5a and 5b. Planets beyond a certain distance are too far away to be affected by tides (see Appendix A). Planets below $10^{-2} M_J$ are not massive enough to be affected by tidal forces and their orbits undergo a purely adiabatic expansion, as shown by the vertical portion of the boundary in Figure 5a.

3.3 Predictions for the number of planets *Gaia* will detect around white dwarfs

The best white dwarf candidates for finding planets are bright (smaller noise) and close (larger signal). $60 \pm 20\%$ of planet detections occur around white dwarfs brighter than $G_{\text{mag}} = 15$, even though they comprise just 326 out of the 152,618 stars in the catalogue. There are far fewer white dwarfs where detection of a close in Jupiter mass planet is likely compared to a $13 M_J$ planet at large semi-major axes (36 compared to 3770) as demonstrated in Figure 6. The two example planets in this figure correspond to some of the smallest ($1 M_J$ at 2 au) and largest ($13 M_J$ at 3.91 au) signals for which there is $S/N > 3$ (almost 100% detection probability). For $1 M_J$ planets there are no $S/N > 3$ candidates with magnitudes greater than 14.5 and beyond 30 pc. These high detection probability candidates are discussed further in Appendix C.

We predict *Gaia* will detect 6 ± 1 planets around white dwarfs that evolve due to mass loss and tides post-main sequence. Of these planets $8 \pm 3\%$ will lie inside 3 au (i.e. at most one), $90 \pm 20\%$ will lie between 3 – 3.91 au. $30 \pm 10\%$ will be less massive than Jupiter. The predicted distribution of planets *Gaia* can detect is shown in Figure 7. We predict *Gaia* will not be able detect planets less massive than $0.13 M_J$ or with semi-major axes less than 1.6 au. The faded region corresponds to planets with non-zero detection probabilities, but which have periods longer than the *Gaia* extended mission length. The orbital parameters of these planets cannot be recovered reliably (Ranalli et al. 2018) so they are not included in the final predicted number of planet detections and the maximum semi-major axis where *Gaia* can detect planets is 3.91 au (for a $0.6 M_{\odot}$ white dwarf). The detected planets are concentrated at the largest masses and semi-major axes, because they have the strongest signals. Comparison with

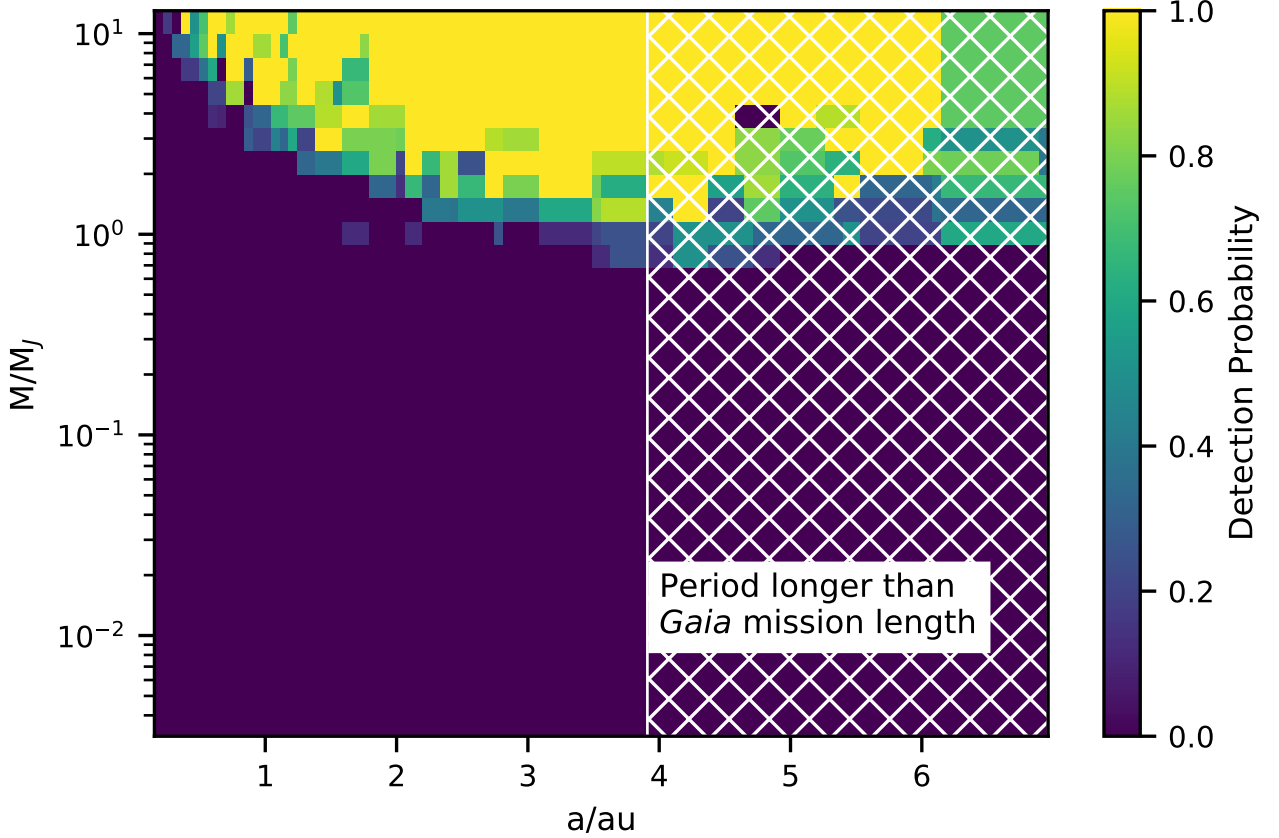


Figure 3. Detection probability, p_{ijk} as a function of mass and semi-major axis for an example $G_{\text{mag}} = 15$ white dwarf at 30 pc . Here detection probability refers to the likelihood of detecting a given planet if it exists around the white dwarf and does not account for $\frac{d^2 N_{\text{WD}}}{da d \log M}$. The hatched region indicates semi-major axes which have non-zero detection probabilities, but periods longer than the mission length. The dark square around 4.5 au and $3 M_J$ results from the stochastic method to determine the detection probabilities in (Ranalli et al. 2018). Almost all planets above $3 M_J$ at a few au will be detected, whilst almost no planets less massive than Jupiter will be detected.

Figure 5a highlights that *Gaia* will not detect any of the low mass planets which should exist around white dwarfs, because they are below the *Gaia* detection threshold.

4 DISCUSSION

This work makes two key predictions: the number and distribution of planets *Gaia* will find around white dwarfs that have evolved from the main-sequence by tides and mass loss. We predict *Gaia* will find 6 ± 1 planets between $1.6 - 3.91\text{ au}$ with masses between $0.03 - 13 M_J$. Whilst the broad form of the distribution (mass and semi-major axis of discovered planets) is robust, the exact numbers of predicted planet detections depend crucially on the chosen main-sequence planet occurrence rate, the adopted post-main sequence planetary system evolution model and the ten year period cut-off for detected planets.

Nonetheless, we consider the numbers to be sufficiently reliable to be used as a benchmark comparison with *Gaia* exoplanet detections in order to determine how important photoevaporation, common envelope evolution and dynamical scattering inwards are for planets around white dwarfs.

4.1 Validity of results

4.1.1 Post-main sequence planetary evolution model

This work focuses only on the effects of stellar mass loss and tidal evolution on the fate of planets post-main sequence Mustill & Villaver (2012). Crucially, two processes are neglected which could potentially lead to planets on orbits interior to 1.6 au , the innermost orbit predicted by tidal evolution in this work. Firstly, planets may survive inside and subsequently escape from the stellar envelope (common envelope evolution Paczynski 1976). While traditional common-envelope models predict a minimum mass of $10 M_J$ for the smallest planets that can survive common-envelope evolution (e.g., Nordhaus et al. 2010), the orbit of the Jupiter-mass planet WD 1856b can be explained by models that incorporate re-ionisation energy or successive engulfment events (Lagos et al. 2021; Chamandy et al. 2021). Common envelope evolution could drastically shrink the orbit, making the planet invisible to astrometry (but more detectable by the transit method). Secondly, multi-planet interactions or Kozai-Lidov interactions with stellar companions can lead to planets scattered inwards post-main sequence stellar evolution, as suggested by Ronco et al. (2020); O’Connor et al.

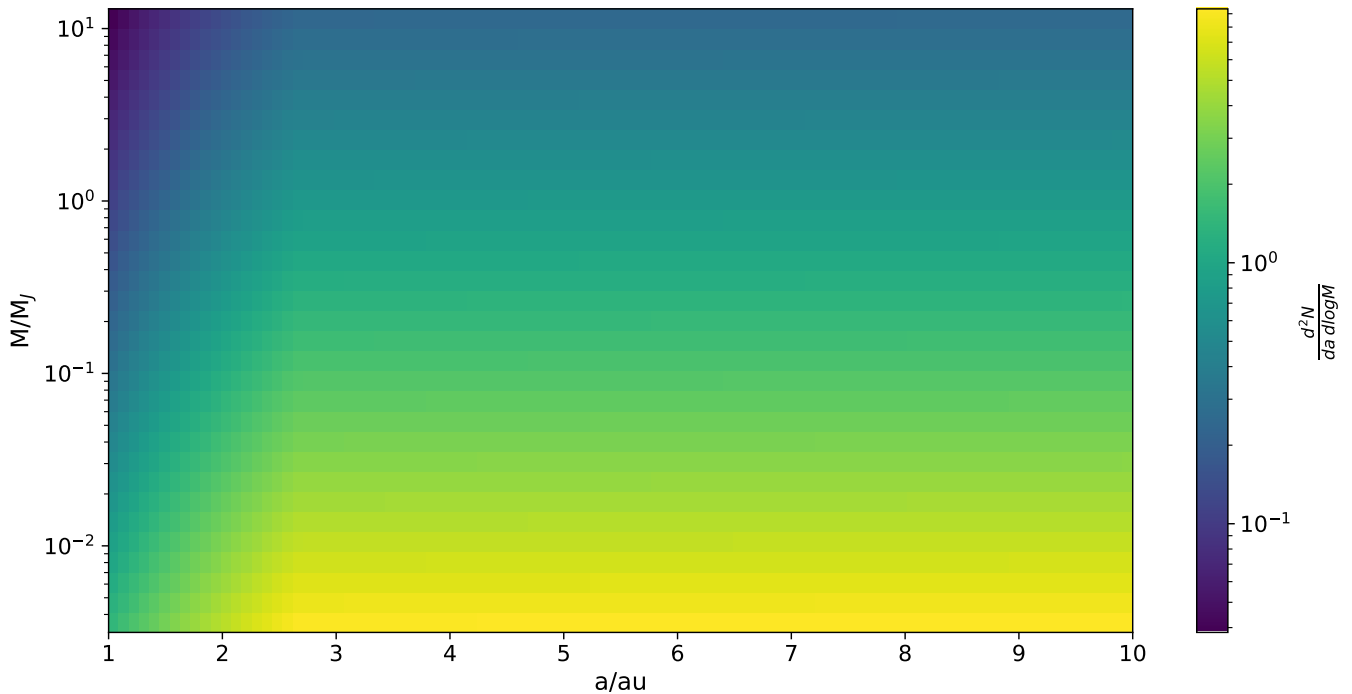


Figure 4. Number of planets per semi-major axis and log M bin ($\frac{d^2 N_{\text{MS}}}{da d \log M}$) for main-sequence stars from [Fernandes et al. \(2019\)](#). Lower mass planets are more common.

(2021); [Stephan et al. \(2021\)](#), amongst others. In the absence of tidal forces, scattering can decrease the semi-major axis by up to a factor of 2 ([Mustill et al. 2014](#), Fig. 6). The potential detection of planets interior to 1.6 au provides an important test of the importance of common envelope evolution and/or dynamical scattering.

The model also neglects photoevaporation, high stellar luminosity heating the planet’s gaseous envelope such that it escapes, which could reduce a planet’s size below the *Gaia* observable limit ([Villaver & Livio 2007](#)). [Villaver & Livio \(2007\)](#) predict a strong dependence of photoevaporation on the planet’s mass and orbital properties. $1M_J$ planets initially within 2 au of their $1M_\odot$ progenitor host star lose 50% of their envelopes, whilst $5M_J$ planets initially at 3 au only lost 0.4-5% of their envelope. Whilst the predicted *Gaia* planet detections will suffer from small number statistics, if there is a lack of detections of $M_P \leq M_J$ planets it could be an indication that photoevaporation is important in these systems.

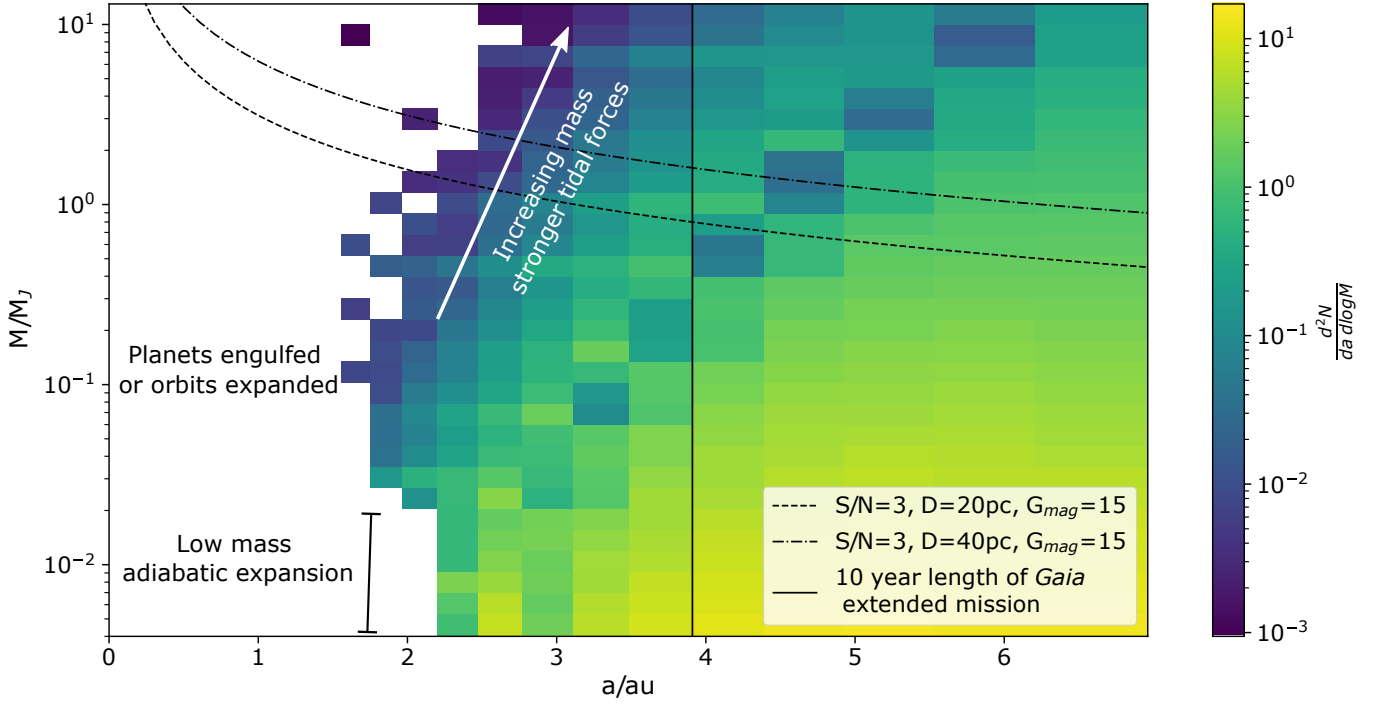
This work models tidal forces as the dissipation of an equilibrium tide by means of convective turbulence in the giant star’s envelope ([Mustill & Villaver 2012](#); [Zahn 1977](#)). The strength of this tide and scalings in the model (especially the dependence on tidal strength with the forcing frequency, i.e., the mean motion) are debated (see, e.g., [Goldreich & Nicholson 1977](#); [Zahn 1977](#); [Penev et al. 2009](#); [Ogilvie & Lesur 2012](#); [Ogilvie 2014](#)). [Mustill & Villaver \(2012\)](#) found that the maximum orbital radius for engulfment can change by up to 1 au for reasonable changes in these parameters. In principle, if we better understood the progenitor population of giant planets, detection of planets around white dwarfs could be used to better constrain the tidal models. Unfortunately however, the number of planets *Gaia* will detect around white dwarfs will be too small for this.

Another potential limitation to the models is the number of simulated planets. Increasing the number of simulated planets would reduce the fractional error on R_{ijk} , since $\sigma(R_{ijk})$ is Poissonian. This would be most significant for bins closest to the star, where the number of planets surviving in each bin is smallest. However, the predicted number of planet detections inside 3 au is so low that increased resolution in this region would be an unnecessary computational expense. The number of planets per bin in the simulations sufficiently resolves the structure in the white dwarf planet distribution.

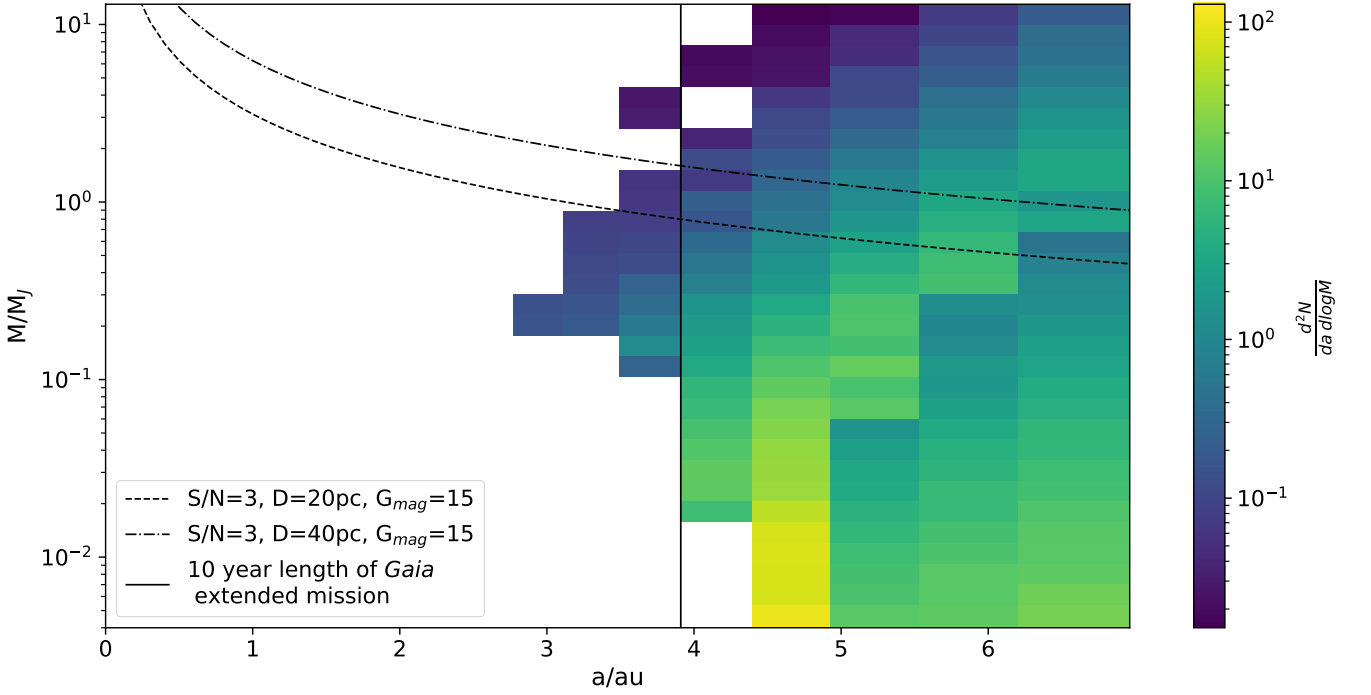
4.1.2 Planet occurrence rate

The main-sequence planet occurrence rate contributes the most to the uncertainties in the predicted number of detected planets (see §2.3.3). However, once *Gaia* exoplanet detections are available for main-sequence stars, these will allow predictions for the number of planets *Gaia* detect to be updated. This will further enable the use of the *Gaia* white dwarf exoplanets to investigate the processes affecting planets’ orbital evolution discussed in §4.1.1.

Our chosen main-sequence planet occurrence rate from [Fernandes et al. \(2019\)](#) crucially accounts for non-detections when calculating the planet occurrence rate by weighting the sum over the number of detected planets by the inverse of survey completeness at the mass and semi-major axis of each planet (see Equation 1 in [Fernandes et al. 2019](#)). However, estimates of completeness are still limited by the lack of planet observations beyond 1 au where most *Gaia* planet detections will lie. Short period planets are easily observed by the transit method and have been surveyed extensively by Kepler and TESS ([Fulton et al. 2017](#); [Petigura et al. 2017](#)). Planets beyond 1 au have been discovered by radial velocity mea-



(a) $1 M_{\odot}$ progenitor. A small proportion of planets survive inside the detection region to the white dwarf phase (see §3.2).



(b) $1.5 M_{\odot}$ progenitor. Stronger tidal effects and greater mass loss means fewer planets survive inside the detection region compared to the $1 M_{\odot}$ progenitor.

Figure 5. Predicted number of planets per semi-major axis and $\log M$ bin ($\frac{d^2 N_{WD}}{da d \log M}$) around a white dwarf with a $1 M_{\odot}$ and $1.5 M_{\odot}$ progenitor. This is based on the evolution of an initial distribution around main-sequence stars ((Fernandes et al. 2019) see Fig 4) taking into account tidal evolution, mass loss and engulfment by the AGB star (see §2.2 for further details). The semi-major axis bins have variable width corresponding to equispaced period bins from (Ranalli et al. 2018) and have average width 0.21 au . The mass bins are 0.12 wide in $\log(M/M_J)$. The solid black line denotes the semi-major axis with a period equal to the length of the *Gaia* extended mission for a planet orbiting a $0.6 M_{\odot}$ white dwarf. The orbital parameters of planets at semi-major axes greater than this cannot be recovered accurately. The dashed and dot-dashed lines represent the detection cut off for a signal-to-noise of three for a $G_{\text{mag}} = 15$ white dwarf at 20 pc and 40 pc respectively. Trends discussed in §3.2 have been labelled on Figure 5a.

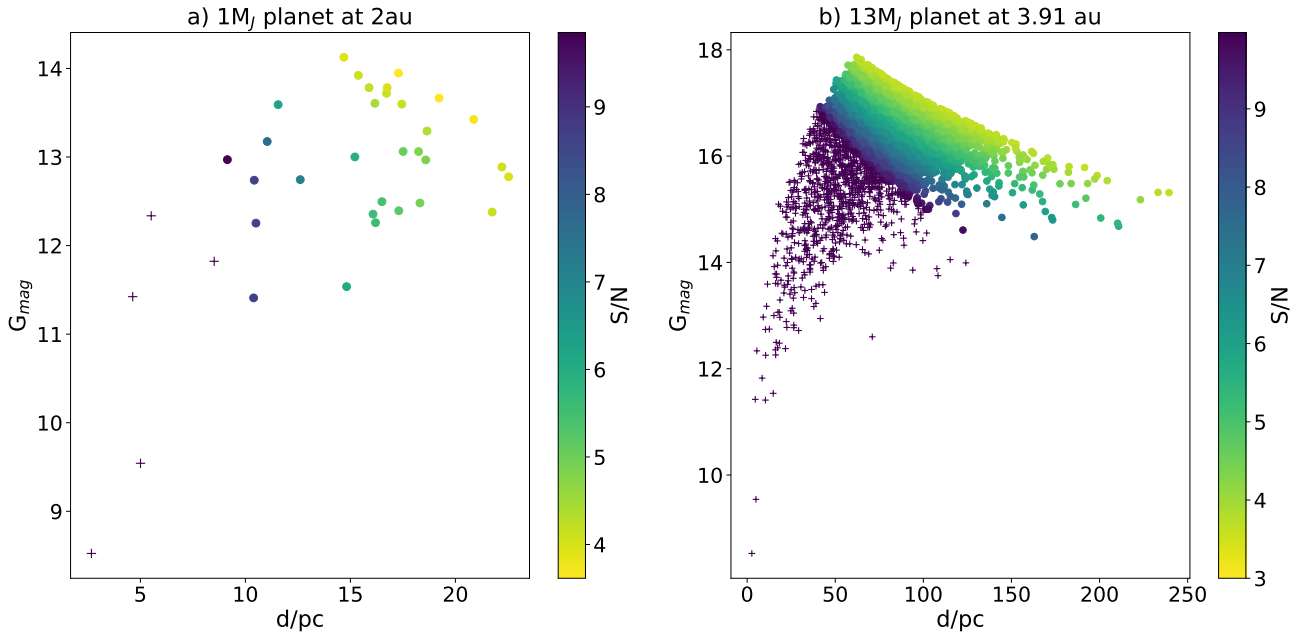


Figure 6. The properties of the white dwarfs (G_{mag} and distance) for whom detection of a $1 M_J$ at 2 au (weak signal) and a $13 M_J$ at 3.9 au is guaranteed if that planet exists around those white dwarfs (detection probability = 1). Candidates with $S/N > 10$ are denoted by the purple +. There are an far fewer candidates, 3 (see Appendix C), for detecting lower mass ($\sim M_J$) close in ($< 2 \text{ au}$) compared to 3770 for a $13 M_J$ planet at 3.91 au . Also note the difference in semi-major axis and G_{mag} scales between the two plots.

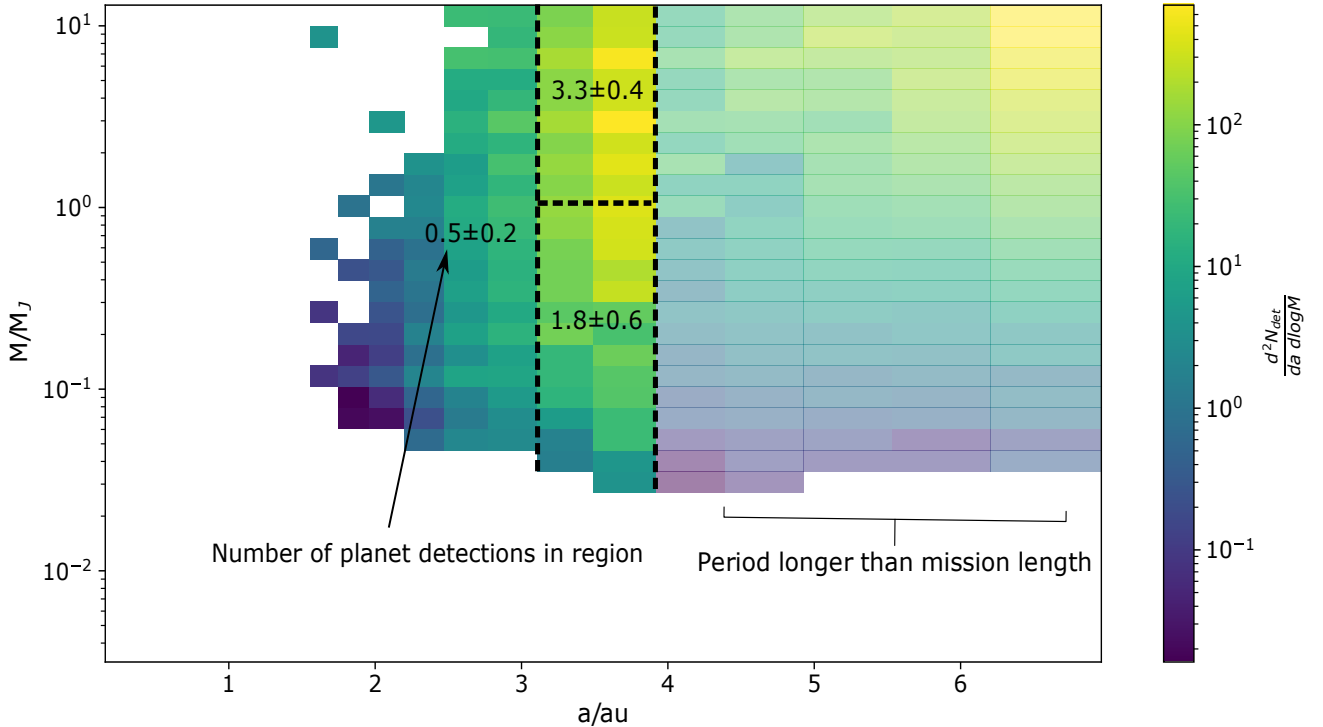


Figure 7. Predicted number of detected planets per semi-major axis and log M bin ($\frac{d^2 N_{\text{det}}}{da d \log M}$). Summing over the distribution gives the total number of planets we predict *Gaia* will detect. The number of planets that we predict will be detected in each region is written in black. The vertical dashed boundary is at $a = 3 \text{ au}$ and the horizontal dashed boundary is at $M = M_J$. The faded region corresponds to planets with periods longer than the extended mission length, which have non-zero detection probabilities, but for which orbital parameters cannot be accurately recovered. For periods longer than the extended mission length, detection probability also decreases so there is a fall off in $\frac{d^2 N_{\text{det}}}{da d \log M}$. No planets less massive than $0.03 M_J$ or interior to 1.6 au will be detected. The gaps and isolated non-zero bins at small semi-major axes result from difference in tidal effects for planets at different semi-major axes motion of planets during post-main sequence evolution (see gaps in Figure 5a).

measurements e.g. Mayor et al. (2011); Wittenmyer et al. (2016), microlensing e.g. Gaudi (2012) and direct imaging e.g. Biller et al. (2013), but these are limited in number, relative to close-in planets.

4.1.3 Probing planets with periods longer than the Gaia mission length

In order to unambiguously detect and characterise the orbit of a planet, multiple orbital periods must be observed. This necessarily limits *Gaia* to planets with periods shorter than the ten year mission length (interior to 3.91 au). However, techniques exist to probe the population of planets on longer periods, based on astrometric detection of fractional orbital periods (see e.g. Penoyre et al. 2020). The faded region in Figure 7 predicts that a substantial population (110 ± 50) of planets evolved from the main-sequence orbit white dwarfs in the four to eight au region, where significant astrometric signals would be detected by *Gaia*, corresponding to fractional orbital periods only. These planets have not been included in the predicted detected population in this work, but these planets would provide a population to compare in detail with individual post-main sequence planetary evolution models similar to comparisons of the Kepler radius valley with photoevaporation models e.g. (Owen & Wu 2017). These planets would be sufficient in number that it becomes possible to investigate how planet occurrence rate changes between more massive, early main-sequence stars (which have now reached the white dwarf phase) and lower mass main-sequence stars.

4.1.4 Planets only survive around higher mass progenitors on orbital periods longer than the Gaia mission length

Figure 5b shows that planets end up beyond *Gaia* detection limit in planetary systems with high mass progenitors. This is because the star loses a higher proportion of its mass and has stronger tidal forces. In this work, we attempt to account for the initial mass of the white dwarf progenitors, by using an initial-final mass relationship to determine which white dwarfs had high mass progenitors. No detectable planets are found around white dwarfs with initial masses higher than $1.5 M_{\odot}$, which using Cummings et al. (2018) corresponds to a final mass of $M = 0.609 \pm 0.054 M_{\odot}$.

In practice, this meant that white dwarfs with masses higher than $0.663 M_{\odot}$ were not included in the analysis presented in §2.3. However, this mass cut off introduces uncertainty in the predicted number of detected planets, because there is error associated with the initial final mass relation and the mass values in the catalogue.

The mixed masses from the Gentile Fusillo et al. (2021) catalogue were used in this work. These were derived by fitting white dwarf atmospheric models and evolutionary sequences to *Gaia* photometry and photometric estimates of $\log g$ and T_{eff} to obtain best fit values of mass and radius. Reddening for white dwarfs beyond 100 pc was corrected for in the mass calculations. These estimates are unreliable for very high ($> 1.3 M_{\odot}$) or very low masses ($< 0.2 M_{\odot}$), but this is not a problem for the mass cut off as the very lowest masses are not underestimated enough to need excluding from the sample and the highest masses are far above the cut off. Using only *Gaia* photometry introduces error in these

masses, because as discussed in Bergeron et al. (2019) due to the high temperatures of white dwarfs it is important to include ‘bluer’ photometry such as SDSS ‘u’ to constrain the peak of the blackbody curve and the value of T_{eff} .

In order to predict which white dwarfs would have no planets on orbital periods shorter than the *Gaia* mission length due to their high progenitor masses, it is necessary to deduce their evolutionary pathway and initial mass based on current observed properties, notably their mass ($\log g$). For this process, we utilise initial to final mass relations which are notoriously unreliable. Uncertainties arise because two stellar models of different initial masses and metallicities or run through different stellar evolution codes can have the same final mass and it is difficult to obtain the metallicity of the progenitor mass from observations. In this work we used the Cummings et al. (2018) MIST-based initial-final mass relation based on stellar clusters, but the difference to the resulting predicted planet population if another relation e.g. (El-Badry et al. 2018; Barrientos & Chanamé 2021) were used is small.

The resolution of the post-main sequence stellar evolution models is also limited to $0.5 M_{\odot}$ differences in progenitor mass. However, the slope of the initial final mass relation in the $1 - 1.5 M_{\odot}$ progenitor range is so shallow and error on the relation so large that this outweighs the uncertainty due to model resolution.

The multiple sources of uncertainty on the mass cut off do not have a significant effect on the results, because the large number of white dwarfs mean the resulting fractional change in catalogue size is small. Repeating the analysis in this work using one and three σ bounds on the white dwarf masses and the cut off value from the initial final mass relation to increase and decrease the number of white dwarfs in the catalogue do not change our results within the errors. Aside from the mathematics of the cut off, there is also uncertainty due to its initial validity. If we discover planets around white dwarfs with higher mass progenitors it suggests these planets have been scattered inwards or these white dwarfs have had a different evolutionary pathway. For example, if a white dwarf underwent a merger, the planetary systems may have a complex history, that proceeds in quite a different manner to the simple picture of tidal evolution presented in this work.

4.1.5 Other limitations

In addition to the effects discussed above the *Gaia* detection probabilities, the predicted magnitude of *Gaia* DR5 errors and the width of the bins in mass-semi-major-axis space will have minor effects on the predicted number of planet detections. The *Gaia* errors used in this work are predictions for DR5 based on eDR3 and we acknowledge this may be updated for future data releases. As the errors decrease with every data release this may lower the mass detection threshold. Revised detection probabilities may also change the exact number of detected planets.

4.2 Significance of the results

This paper highlights the importance of *Gaia* for the detection of exoplanets on medium orbital periods across the HR-diagram (Perryman et al. 2014). White dwarf exoplanets are

key to investigating the effects of stellar evolution on planetary systems. Whilst planetary systems around white dwarfs have been hypothesised for years to explain white dwarf pollution (Jura & Young 2014), there are few known planets (Vanderburg et al. 2020; Blackman et al. 2021; Luhman et al. 2011). Many unsuccessful surveys have searched for close-in planets orbiting white dwarfs (e.g. Faedi et al. 2011; Agol 2011; Burleigh et al. 2002), but no current techniques are sensitive to planets on wide (year) orbits. This work highlights how *Gaia* will shed light on these important planetary systems.

Predictions are made for the planet population around white dwarfs, based on the evolution of the currently known main-sequence planet population due to tides and stellar mass loss, resulting in 6 ± 1 planets detectable by *Gaia*. Notably, no planets are predicted interior to 1.6 au , where they should have been engulfed by their host star, providing a test for the importance of common envelope evolution or dynamical scattering in the post-main sequence evolution of planetary systems. If we see fewer Jupiter mass planets than expected it suggests they may be removed by photoevaporation. Existing observations and theoretical work (e.g. Veras 2016; Vanderburg et al. 2020; Muñoz & Petrovich 2020; Veras & Gänsicke 2015; Villaver & Livio 2007; Alonso et al. 2021; Lagos et al. 2021) already suggest these processes could be important. If more planets are seen than expected it could provide evidence for second-generation planet formation. Predicting a distribution of planets unaffected by these processes can help us confirm which detected planets result from these processes and can be used to test models of these mechanisms.

The results in this paper are broadly inline with previous work. The number of planet detections (6 ± 1) predicted by this paper is slightly lower than the 13 predicted by Perryman et al. (2014). Perryman et al. (2014) used the final mass of the white dwarf in a main-sequence planet occurrence rate, which may have overestimated the number of planets around white dwarfs in the *Gaia* observable range, because it did not account for the expansion of planetary orbits and the engulfment of planets during post-main sequence stellar evolution. The mass detection threshold, $0.03 \pm 0.004 M_J$, is also lower than previous work ($2 M_J$ Silvotti et al. (2011)). We attribute this to improved estimates of *Gaia* errors and an enlarged catalogue of known white dwarfs. The lowest mass planets can only be found around the closest white dwarfs: including white dwarfs within 13 pc lowers the mass detection threshold from $0.15 M_J$ to $0.03 M_J$.

4.3 Outer planets and the link with metals observed in the atmosphere of white dwarfs

Observations of polluted white dwarfs provide the best means of studying outer planetary systems to date. Most theories to explain the presence of metals in the atmospheres of white dwarfs suggest that material is scattered inwards from an outer planetary system that survived the star's evolution (Farihi 2016). The planets that *Gaia* will detect provide a crucial piece of the puzzle: for the first time it will be possible to probe the outer planets orbiting white dwarfs. Here, we highlight that a link between the *Gaia* planet detections and metals in the atmospheres of white dwarfs is not straightforward and a one:one correlation is not anticipated.

In order to investigate a potential link between *Gaia* planet

detections and asteroids or comets scattered inwards to pollute white dwarfs, we consider a simple scenario. Planets on the inner edges of planetesimal belts can scatter planetesimals and their ability to scatter planetesimals can increase following stellar mass loss. Many scattered bodies are ejected, but some can be scattered inwards, potentially ending up on star-grazing orbits close to the white dwarf (Bonsor et al. 2011; Frewen & Hansen 2014; Debes et al. 2012). Interior planets may be required to scatter planets along a chain (Marino et al. 2018). Many of the planets detected by *Gaia* migrate less than expected from an adiabatic expansion due to stellar mass loss due to the effects of tides. If the planetary body directly exterior to them, be it a planet or a planetesimal belt, migrates outwards adiabatically, a dynamical 'gap' in the planetary system is created, across which it becomes harder to scatter bodies inwards. Here we highlight that many planets detected by *Gaia* will have created such dynamical 'gaps' in their planetary systems, making the scattering of material inwards harder, and thus, the pollution of their host stars less likely.

To assess which planets in the predicted white dwarf planet distribution could contribute to white dwarf pollution we grouped the simulated planets into four categories (see Figure 8): planets engulfed by the star, planets that migrated outwards adiabatically and could scatter material from an outer planetesimal belt and planets whose orbits were influenced additionally by tides, either migrating inwards or outwards (less far than adiabatically). Whilst the inward migrating planets are less likely to be part of a planet chain scattering material onto the white dwarf from the outer planetary system, they could potentially interact with rocky material interior to their initial orbit, if the material migrates outwards adiabatically. For the mathematics of the categorisation see Appendix B.

Almost all surviving planets in the *Gaia* detection region have dynamical 'gaps' in their planetary systems. This is shown in Figure 8, where only purple and green points lie above the *Gaia* detection curves and inside 3.91 au . All planets that migrate outwards adiabatically and could readily pollute white dwarfs by scattering material inwards lie beyond 3.91 au and most of them are not massive enough to be detected. Even if *Gaia* detects Jupiter mass planets that have migrated inwards, they are unlikely to be responsible for scattering planetary material from an outer system inwards. The detected Jupiters will have migrated inwards, separating themselves dynamically from the outer system. Additionally, Jupiter mass planets are more efficient at ejecting material from a planetary system than scattering it inwards (Wyatt et al. 2017). They also scatter material too rapidly to give the observed long-term accretion of material onto some white dwarfs (Mustill et al. 2018). Low mass planets are more likely to be a long term source of pollution in a planetary system, because they scatter more material inwards and do so more slowly than Jupiter (Mustill et al. 2018; O'Connor et al. 2021). These low mass planets are not detectable by *Gaia*. Therefore, white dwarfs with *Gaia* detected planets are less likely to be polluted than other white dwarfs with lower mass planets, that *Gaia* does not detect. This is an important result: if *Gaia* does not find a correlation between detected planets and polluted white dwarfs, this does not rule out the possibility that planets pollute white dwarfs.

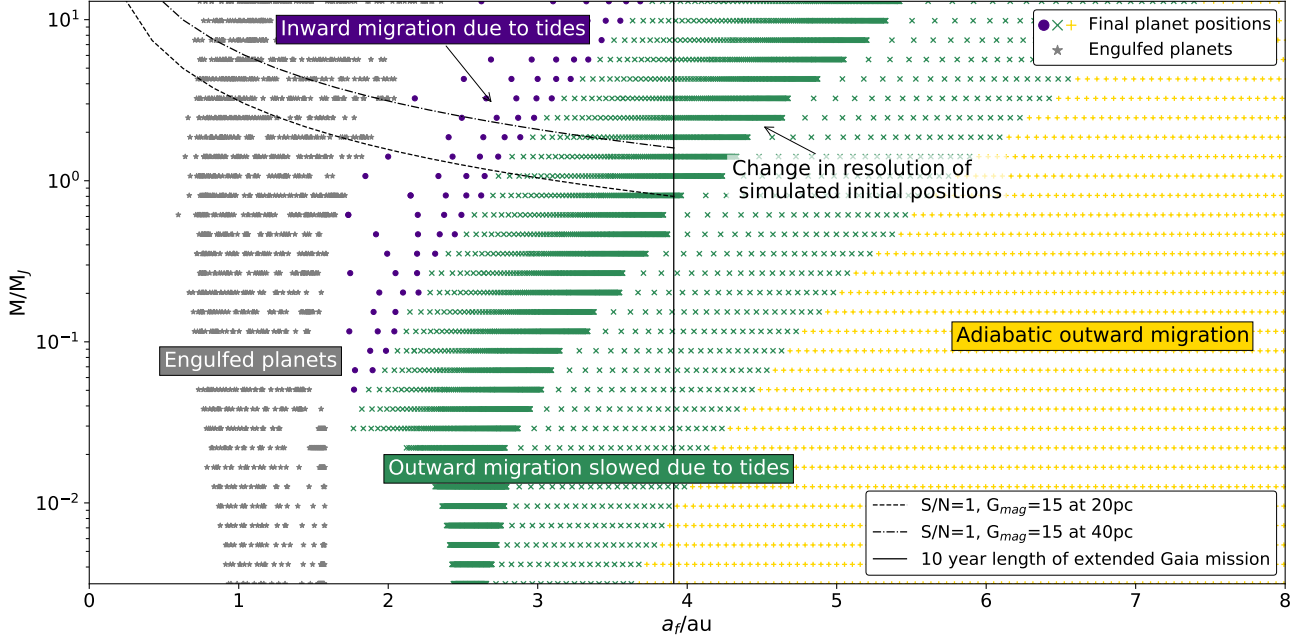


Figure 8. Final positions of simulated planets plotted as a function of their final semi-major axis and mass colour coded according to whether or not they could scatter material onto a white dwarf (see §4.3). Engulfed planets are shown by the grey stars, inward migrating planets by the purple circles, planets moving outward adiabatically where material could be scattered from an outer planetesimal belt by the yellow pluses and outward moving planets with a dynamical ‘gap’ in their system due to the effects of tides by the green crosses. The minimum planet mass detected as a function of semi-major axis for $S/N = 1$ for a $G_{\text{mag}} = 15$ white dwarf at 20 pc and 40 pc shown by the black dashed and dotted lines. The solid vertical line indicates the period cut off due to the length of the extended *Gaia* mission.

5 CONCLUSION

Gaia is revolutionary for almost every field in astrophysics, and exoplanets is no exception. Astrometric detection of wide-orbit (few au) planets orbiting stars across the HR diagram by *Gaia* will uniquely probe the outer regions of planetary systems, crucially linked to the habitable zone around sun-like stars, such as our own. *Gaia* planet detections around white dwarfs will probe the fate of planetary systems, providing secure evidence as to the key processes that influence planets post-main sequence.

This work predicts that *Gaia* will detect 6 ± 1 white dwarf exoplanets that evolved from the main-sequence only due to tides and the mass loss of the host star during post-main sequence evolution. These planets will have masses $0.03 - 13 M_J$ and semi-major axes $1.6 - 3.91 \text{ au}$. Comparison of these predictions with the *Gaia* white dwarf planet detections will tell us how important dynamical scattering, common envelope evolution and photo-evaporation are. Notably, any planets detected interior to 1.6 au , or around stars with progenitors more massive than $1.5 M_\odot$ must have been subject to additional processes post-main sequence.

Metals observed in the atmospheres of white dwarfs are commonly linked to outer planetary systems, in particular, comets or asteroids scattered inwards by planets. This work highlights how many white dwarfs planets detected by *Gaia* will have evolved due to tides, leaving dynamical gaps in their outer planetary systems. These gaps render the scattering inwards of material to pollute the white dwarf harder. White dwarf pollution may, therefore, be more commonly associated with lower mass outer planets, hidden from *Gaia* astrometry.

6 ACKNOWLEDGEMENTS

We would like to thank Piero Ranalli for sharing the exact values of his detection probabilities from [Ranalli et al. \(2018\)](#). We would also like to thank Laura Rogers, Zephyr Penoyre, Marc Brouwers, Andy Buchan, Elliot Lynch, Mark Wyatt and Rachel Fernandes for their helpful discussions. AJM acknowledges support from the Swedish Research Council (grant 2017-04945). AB acknowledges funding from a Royal Society Dorothy Hodgkin Research Fellowship, DH150130 and a Royal Society University Research Fellowship, URF\R1\211421. HS acknowledges funding on a NERC studentship NE/S007474/1. For the purpose of open access, the authors have applied a Creative Commons Attribution (CC BY) licence to any Author Accepted Manuscript version arising.

7 DATA AVAILABILITY

Additional data and the code used in this publication are available on Github at <https://github.com/Hannah-RS/Gaia-white-dwarf>. The table of white dwarf candidates in Appendix C will be available on Vizier after publication.

REFERENCES

- Agol E., 2011, *The Astrophysical Journal*, 731, L31
 Alonso R., et al., 2021, *Astronomy & Astrophysics, Volume 649, id.A131, <NUMPAGES>12</NUMPAGES> pp.*, 649, A131

- Bailer-Jones C. A. L., Rybizki J., Fouesneau M., Demleitner M., Andrae R., 2021, *The Astronomical Journal*, 161, 147
- Barker A. J., 2020, *Monthly Notices of the Royal Astronomical Society*, 498, 2270
- Barnes R., Quinn T., 2004, *The Astrophysical Journal*, 611, 494
- Barrientos M., Chanamé J., 2021, *The Astrophysical Journal*, 923, 181
- Bear E., Soker N., 2011, *Monthly Notices of the Royal Astronomical Society*, 414, 1788
- Belokurov V., et al., 2020, *Monthly Notices of the Royal Astronomical Society*, 496, 1922
- Bergeron P., Dufour P., Fontaine G., Coutu S., Blouin S., Genest-Beaulieu C., Bédard A., Rolland B., 2019, *The Astrophysical Journal*, 876, 67
- Bertolami M. M. M., 2018, *Proceedings of the International Astronomical Union*, 14, 36
- Biller B. A., et al., 2013, *The Astrophysical Journal*, 777, 160
- Blackman J. W., et al., 2021, *Nature*, 598, 272
- Bonsor A., Mustill A. J., Wyatt M. C., 2011, *Monthly Notices of the Royal Astronomical Society*, 414, 930
- Bryan M. L., et al., 2016, *The Astrophysical Journal*, 821, 89
- Burleigh M. R., Clarke F. J., Hodgkin S. T., 2002, *Monthly Notices of the Royal Astronomical Society*, 331, L41
- Casertano S., et al., 2008, *Astronomy & Astrophysics*, 482, 699
- Chamandy L., Blackman E. G., Nordhaus J., Wilson E., 2021, *Monthly Notices of the Royal Astronomical Society: Letters*, 502, L110
- Chiang E., Kite E., Kalas P., Graham J. R., Clampin M., 2009, *The Astrophysical Journal*, 693, 734
- Collaboration G., et al., 2020, eprint arXiv:2012.02036, p. arXiv:2012.02036
- Cumming A., Butler R. P., Marcy G. W., Vogt S. S., Wright J. T., Fischer D. A., 2008, *Publications of the Astronomical Society of the Pacific*, 120, 531
- Cummings J. D., Kalirai J. S., Tremblay P.-E., Ramirez-Ruiz E., Choi J., 2018, *The Astrophysical Journal*, 866, 21
- Dawson R. I., 2018, in Deeg H. J., Belmonte J. A., eds., *Handbook of Exoplanets*. p. 114, doi:10.1007/978-3-319-55333-7_114
- Debes J. H., Sigurdsson S., Woodgate B. E., 2005, *The Astrophysical Journal*, 633, 1168
- Debes J. H., Walsh K. J., Stark C., 2012, *The Astrophysical Journal*, 747, 148
- Dufour P., Blouin S., Coutu S., Fortin-Archambault M., Thibeault C., Bergeron P., Fontaine G., 2017, 20th European White Dwarf Workshop, 509, 3
- El-Badry K., Rix H.-W., Weisz D. R., 2018, *The Astrophysical Journal*, 860, L17
- Faedi F., West R. G., Burleigh M. R., Goad M. R., Hebb L., 2011, *Monthly Notices of the Royal Astronomical Society*, 410, 899
- Farihi J., 2016, *New Astronomy Reviews*, 71, 9
- Farihi J., Wyatt M. C., Greaves J. S., Bonsor A., Sibthorpe B., Panić O., 2014, *Monthly Notices of the Royal Astronomical Society*, 444, 1821
- Fernandes R. B., Mulders G. D., Pascucci I., Mordasini C., Emsenhuber A., 2019, *The Astrophysical Journal*, 874, 81
- Frewen S. F. N., Hansen B. M. S., 2014, *Monthly Notices of the Royal Astronomical Society*, 439, 2442
- Fulton B. J., et al., 2014, *The Astrophysical Journal*, 796, 114
- Fulton B. J., et al., 2017, *The Astronomical Journal*, 154, 109
- Fulton B. J., et al., 2021, *The Astrophysical Journal Supplement Series*, 255, 14
- Gaia Collaboration et al., 2016, *Astronomy and Astrophysics*, 595, A2
- Gaia Collaboration et al., 2018, *Astronomy and Astrophysics*, 616, A1
- Gaia Collaboration Brown A. G. A., Vallenari A., Prusti T., de Bruijne J. H. J., Babusiaux C., Biermann M., 2020, arXiv e-prints, 2012, arXiv:2012.01533
- Gaudi B. S., 2012, *Annual Review of Astronomy and Astrophysics*, 50, 411
- Gentile Fusillo N. P., et al., 2019, *Monthly Notices of the Royal Astronomical Society*, 482, 4570
- Gentile Fusillo N. P., et al., 2021, *Monthly Notices of the Royal Astronomical Society*, 508, 3877
- Goldreich P., Nicholson P. D., 1977, *Icarus*, 30, 301
- Gould A., Kilic M., 2008, *The Astrophysical Journal*, 673, L75
- Harrison J. H. D., Bonsor A., Madhusudhan N., 2018, *Monthly Notices of the Royal Astronomical Society*, 479, 3814
- Hogan E., Burleigh M. R., Clarke F. J., 2011, *PLANETARY SYSTEMS BEYOND THE MAIN SEQUENCE: Proceedings of the International Conference. AIP Conference Proceedings, Volume 1331, pp. 271-277 (2011)*, 1331, 271
- Hollands M. A., Tremblay P. E., Gänsicke B. T., Gentile-Fusillo N. P., Toonen S., 2018, *Monthly Notices of the Royal Astronomical Society*, 480, 3942
- Ivanova N., et al., 2013, *The Astronomy and Astrophysics Review*, 21, 59
- Jura M., 2003, *The Astrophysical Journal*, 584, L91
- Jura M., Young E., 2014, *Annual Review of Earth and Planetary Sciences*, 42, 45
- Kaltenegger L., MacDonald R. J., Kozakis T., Lewis N. K., Mamajek E. E., McDowell J. C., Vanderburg A., 2020, *The Astrophysical Journal*, 901, L1
- Kervella P., Arenou F., Mignard F., Thévenin F., 2019, *Astronomy and Astrophysics*, 623, A72
- Kervella P., Arenou F., Thévenin F., 2022, *Astronomy & Astrophysics*, 657, A7
- Kuchner M. J., Koresko C. D., Brown M. E., 1998, *The Astrophysical Journal*, 508, L81
- Lagos F., Schreiber M. R., Zorotovic M., Gänsicke B. T., Ronco M. P., Hamers A. S., 2021, *Monthly Notices of the Royal Astronomical Society*, 501, 676
- Loeb A., Maoz D., 2013, *Monthly Notices of the Royal Astronomical Society*, 432, L11
- Luhman K. L., Burgasser A. J., Bochanski J. J., 2011, *The Astrophysical Journal Letters*, 730, L9
- Marino S., Bonsor A., Wyatt M. C., Kral Q., 2018, *Monthly Notices of the Royal Astronomical Society*, 479, 1651
- Matthews L. D., Claussen M. J., 2018, *Science with a Next Generation Very Large Array*, ASP Conference Series, Vol. 517. ASP Monograph 7. Edited by Eric Murphy., p.281, 517, 281
- Mayor M., et al., 2011, arXiv e-prints, 1109, arXiv:1109.2497
- Morbidelli A., Levison H. F., Gomes R., 2008, in Barucci M. A., Boehnhardt H., Cruikshank D. P., Morbidelli A., Dotson R., eds., *The Solar System Beyond Neptune*. p. 275
- Mustill A. J., Villaver E., 2012, *The Astrophysical Journal*, 761, 121
- Mustill A. J., Veras D., Villaver E., 2014, *Monthly Notices of the Royal Astronomical Society*, 437, 1404
- Mustill A. J., Villaver E., Veras D., Gänsicke B. T., Bonsor A., 2018, *Monthly Notices of the Royal Astronomical Society*, 476, 3939
- Muñoz D. J., Petrovich C., 2020, *The Astrophysical Journal Letters*, 904, L3
- Nordhaus J., Spiegel D. S., Ibgui L., Goodman J., Burrows A., 2010, *Monthly Notices of the Royal Astronomical Society*, 408, 631
- Ogilvie G. I., 2014, *Annual Review of Astronomy and Astrophysics*, 52, 171
- Ogilvie G. I., Lesur G., 2012, *Monthly Notices of the Royal Astronomical Society*, 422, 1975
- Owen J. E., Wu Y., 2017, *The Astrophysical Journal*, 847, 29
- O'Connor C. E., Liu B., Lai D., 2021, *Monthly Notices of the Royal Astronomical Society*, 501, 507
- Paczynski B., 1976, *Symposium - International Astronomical Union*, 73, 75

Penev K., Sasselov D., Robinson F., Demarque P., 2009, *ApJ*, **704**, 930
 Penoyre Z., Belokurov V., Wyn Evans N., Everall A., Koposov S. E., 2020, *Monthly Notices of the Royal Astronomical Society*, **495**, 321
 Penoyre Z., Belokurov V., Evans N. W., 2022, *Monthly Notices of the Royal Astronomical Society*, p. stac959
 Perryman M., Hartman J., Bakos G. a., Lindegren L., 2014, *The Astrophysical Journal*, **797**, 14
 Petigura E. A., et al., 2017, *The Astronomical Journal*, **154**, 107
 Ranalli P., Hobbs D., Lindegren L., 2018, *Astronomy & Astrophysics*, **614**, A30
 Ronco M. P., Schreiber M. R., Giuppone C. A., Veras D., Cuadra J., Guilera O. M., 2020, *The Astrophysical Journal Letters*, **898**, L23
 Santerne A., et al., 2016, *Astronomy and Astrophysics*, **587**, A64
 Shannon A., Bonsor A., Kral Q., Matthews E., 2016, *Monthly Notices of the Royal Astronomical Society*, **462**, L116
 Sigurdsson S., Richer H. B., Hansen B. M., Stairs I. H., Thorsett S. E., 2003, *Science*, **301**, 193
 Silvotti R., Sozzetti A., Lattanzi M., 2011, *AIP Conference Proceedings*, **1331**, 336
 Stephan A. P., Naoz S., Gaudi B. S., 2021, *The Astrophysical Journal*, **922**, 4
 Swan A., Kenyon S. J., Farihi J., Dennihy E., Gänsicke B. T., Hermes J. J., Melis C., von Hippel T., 2021, *Monthly Notices of the Royal Astronomical Society*, **506**, 432
 Tokunaga A. T., Becklin E. E., Zuckerman B., 1990, *The Astrophysical Journal*, **358**, L21
 Vanderburg A., et al., 2020, *Nature*, **585**, 363
 Vassiliadis E., Wood P. R., 1993, *ApJ*, **413**, 641
 Veras D., 2016, *Royal Society Open Science*, **3**, 150571
 Veras D., Gänsicke B. T., 2015, *Monthly Notices of the Royal Astronomical Society*, **447**, 1049
 Veras D., Wyatt M. C., Mustill A. J., Bonsor A., Eldridge J. J., 2011, *Monthly Notices of the Royal Astronomical Society*, **417**, 2104
 Veras D., Mustill A. J., Bonsor A., Wyatt M. C., 2013, *Monthly Notices of the Royal Astronomical Society*, **431**, 1686
 Villaver E., Livio M., 2007, *The Astrophysical Journal*, **661**, 1192
 Wisdom J., 1980, *The Astronomical Journal*, **85**, 1122
 Wittemmyer R. A., et al., 2016, *The Astrophysical Journal*, **819**, 28
 Wyatt M. C., Bonsor A., Jackson A. P., Marino S., Shannon A., 2017, *Monthly Notices of the Royal Astronomical Society*, **464**, 3385
 Xu S., Ertel S., Wahhaj Z., Milli J., Scicluna P., Bertrang G. H.-M., 2015, *Astronomy & Astrophysics*, **579**, L8
 Zahn J.-P., 1977, *Astronomy and Astrophysics*, **500**, 121
 Zhu W., Dong S., 2021, arXiv:2103.02127 [astro-ph]
 Zuckerman B., Koester D., Dufour P., Melis C., Klein B., Jura M., 2011, *The Astrophysical Journal*, **739**, 101
 von Hippel T., Thompson S. E., 2007, *The Astrophysical Journal*, **661**, 477

APPENDIX A: EFFECTS OF TIDES

As discussed in §3.2 and §4.1.1 tides have a strong effect on the final position of planets above a certain mass. The strength of this effect can be quantified by f , the ratio of the final position of a planet and the final position expected from an adiabatic expansion:

$$f = \frac{a_f(\text{true})}{a_f(\text{adiabatic})}. \quad (\text{A1})$$

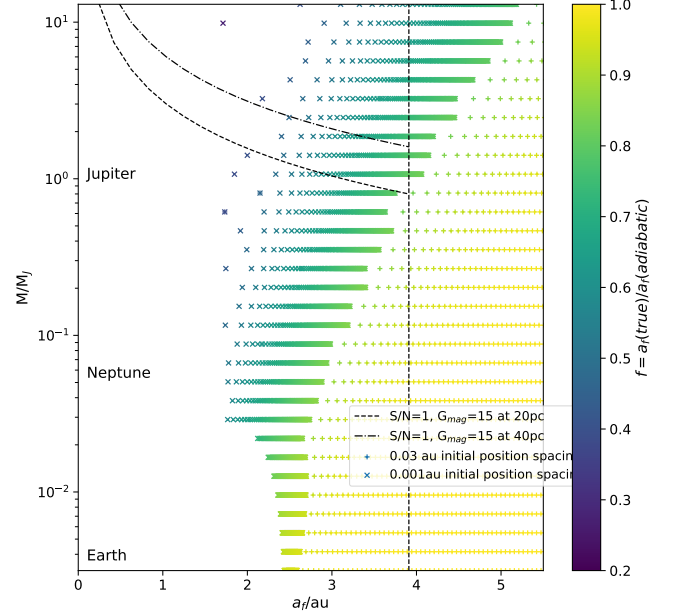


Figure A1. Final positions of simulated planets with periods less than ten years colour coded by $f = \frac{a_f(\text{true})}{a_f(\text{adiabatic})}$. Yellow points indicate planets' orbits which underwent an adiabatic expansion, whilst green to blue points indicate planets affected by tidal forces. Values of $f < 0.57$ indicate the planet moved inwards.

The final position of a planet can be written as

$$a_f = \frac{M_\star(\text{initial})}{M_\star(\text{final})} f a_i = p f a_i. \quad (\text{A2})$$

If $f < \frac{1}{p}$ then $a_f < a_i$ and tidal forces were strong enough that the planet moved inwards. For a $1M_\odot$ star in our simulations $p = 0.5702$. Planets closer to their star experience stronger tidal forces and more massive planets experience tidal forces over a wider range of initial positions, as shown by Figure A1. These tidal forces cause planets with a small range of initial positions (Figure A2) to spread over a wide range of final positions. This contributes to the low number of predicted planet detections, because the semi-major axis range of main-sequence planets which will evolve to have periods less than ten years (the predicted *Gaia* extended mission length) is small.

APPENDIX B: DYNAMICAL GAP CALCULATIONS

For definitions of f and p see Appendix A.

Planetary systems tend on average to be dynamically packed, or in other words the planetary bodies settle down to a stable configuration in which they are sufficiently separated that interactions occur on timescales longer than the lifetime of the system (Barnes & Quinn 2004; Shannon et al. 2016; Dawson 2018). The inner edge of a planetesimal belt can be carved by a planet that is orbiting just interior to it (Chiang et al. 2009), just like Neptune sculpts the inner edge of the Kuiper belt (e.g. Morbidelli et al. 2008). If this is the case, when the star undergoes mass loss, the planetesimals in the belt migrate outwards adiabatically, but the planet interior to the belt may also be influenced by tides from the

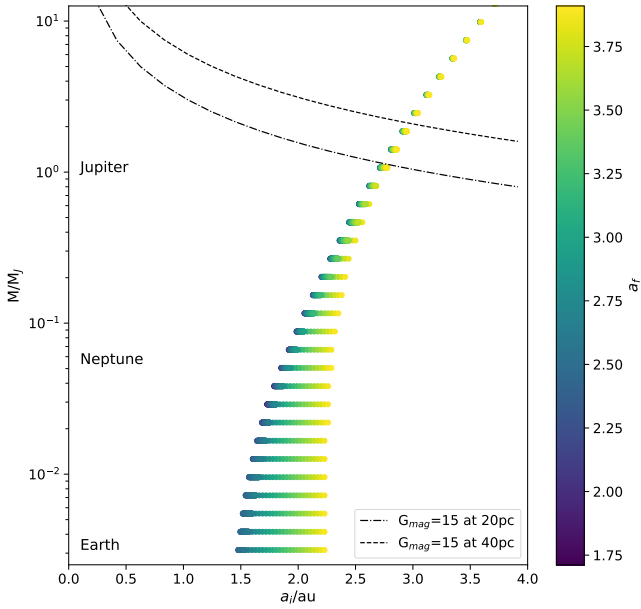


Figure A2. Initial positions of planets with final positions inside the *Gaia* detection region colour-coded by final position.

AGB star. As a result, the planet migrates out more slowly, or even in the opposite direction to the belt. In this scenario, a dynamical gap is created, across which it is harder to scatter planetesimals than in the main-sequence configuration, as discussed in §4.3. The width of this gap can be calculated analytically, by considering the change in the width of a planet's chaotic zone to the orbit of an exterior planetesimal belt undergoing an adiabatic expansion.

The width of this chaotic zone, δa_{chaos} is defined as:

$$\delta a_{chaos} = 1.3 a_{pl} \left(\frac{M_{pl}}{M_*} \right)^{\frac{2}{7}}, \quad (B1)$$

where M_{pl} and M_* are the planet and stellar mass respectively (Wisdom 1980). It extends from the semi-major axis of the planet (a_{pl}) to $a_{pl} \pm \delta a_{chaos}$.

As a star loses mass, the orbit of a planet and the outer edge of its chaotic zone and any surrounding planetesimal belts expand. The inner edge of the planetesimal belt, which is initially at the outer edge of the chaotic zone, a_{in} , expands adiabatically

$$a_{in} = p a_{pl} \left(1 + 1.3 \left(\frac{M_{pl}}{M_*} \right)^{\frac{2}{7}} \right). \quad (B2)$$

The outer edge of the chaotic zone, a_{out} , is affected by the altered planet-star mass ratio and the change in planet semi-major axis.

$$a_{out} = f p a_{pl} \left(1 + 1.3 \left(p \frac{M_{pl}}{M_*} \right)^{\frac{2}{7}} \right). \quad (B3)$$

If the outer edge of the chaotic zone becomes larger than the inner edge of the belt, mass from the belt ends up in the chaotic zone and becomes unstable and can be scattered inwards onto the star. However, if the planet is strongly affected by tidal forces, the outer edge of the chaotic zone expands less than the planetesimal belt and a dynamical ‘gap’ forms in the system. The critical value of f for this scenario

is given in Equation B4.

$$f_{crit} < \frac{1 + 1.3 \left(\frac{M_{pl}}{M_*} \right)^{\frac{2}{7}}}{1 + 1.3 \left(p \frac{M_{pl}}{M_*} \right)^{\frac{2}{7}}}. \quad (B4)$$

In this equation M_* is the **initial** stellar mass. For a Jupiter mass planet and $1M_{\odot}$ progenitor this corresponds to $f < 0.975$ - an almost adiabatic migration. The points in Figure 8 were classified as follows: purple, $f < 0.5702$ (see Appendix A); green, $0.5702 < f < f_{crit}$; yellow, $f > f_{crit}$ and grey, engulfed.

APPENDIX C: HIGH DETECTION PROBABILITY WHITE DWARFS

There are 36 white dwarfs for which the S/N of a $1 M_J$ planet at 2 au is greater than three (Figure 6). These objects are listed in Table C1. Of particular interest is G29-38 - the first polluted white dwarf for which a debris disc was observed (Tokunaga et al. 1990; Jura 2003) and which has variable photospheric calcium line strengths (von Hippel & Thompson 2007). *Gaia* measurements of G29-38 will build on existing observations with Keck, the Hubble Space Telescope, Herschel and ALMA (e.g. Debes et al. 2005; Farihi et al. 2014; Kuchner et al. 1998). These observations currently rule out planets $> 6 M_J$ beyond 12 au and $> 16 M_J$ between 3-12 au (Debes et al. 2005). Farihi et al. (2014) use ALMA and Herschel observations to rule out the presence of dust in the 1-100 au region emitting with $L_{IR}/L_* > 10^{-4}$ from an evolved Kuiper-belt analogue. *Gaia* could rule out the existence of planets above approximately $1 M_J$ between 1-4 au around this star (see Figure C1). A similar figure could be produced for any white dwarf in the catalogue.

This paper has been typeset from a \LaTeX file prepared by the author.

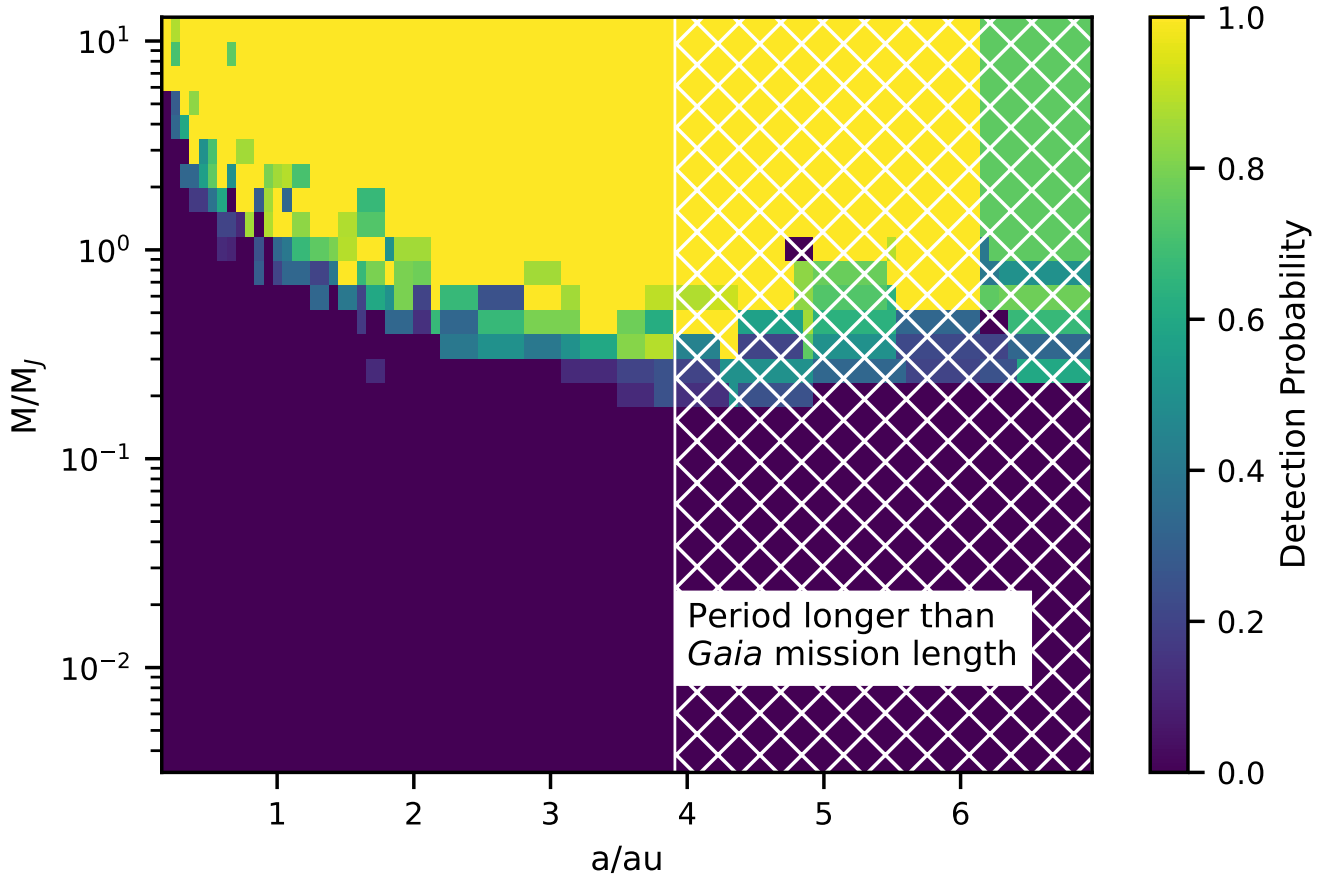


Figure C1. Detection probability, p_{ljk} (§2.1) as a function of mass and semi-major axis for G29-38. Here detection probability refers to the likelihood of detecting a given planet if it exists around G29-38 and does not account for the likelihood of a given planet existing around the star.

White dwarf name	Gaia eDR3 source ID	Distance (pc)	G_{mag}	S/N for $1M_J$ at 2au	error on S/N	Ca/He	Ca/H
WD J064509.30−164300.72	2947050466531873024	2.7	8.5	33.7	5.6		
WD J114542.92−645029.46	5332606522595645952	4.6	11.4	19.4	3.2		
WD J041521.80−073929.20	3195919254111315712	5.0	9.5	18.0	3.0		
WD J043112.57+585841.29	470826482637310848	5.5	12.3	16.3	2.7		
WD J084132.43−325632.92	5639391810273308416	8.5	11.8	10.6	1.8		< -11.12
WD J074020.79−172449.16	5717278911884258176	9.1	13.0	9.8	1.6		
WD J031031.02−683603.38	4646535078125821568	10.4	11.4	8.7	1.4		
WD J120526.67−233312.14	3489719481290397696	10.4	12.7	8.6	1.4		-9.7
WD J192034.92−074000.07	4201781696994073472	10.5	12.3	8.6	1.4		
WD J214241.01+205958.12	1792830060723673472	11.0	13.2	7.7	1.3		
WD J013759.39−045944.67	2480523216087975040	12.6	12.7	7.1	1.2		<-11.53
WD J195629.23−010232.67	4235280071072332672	11.6	13.6	6.2	1.0		<-11.27
WD J203421.89+250349.75	1831553382794173824	14.8	11.5	6.1	1.0		
WD J154730.02−375508.46	6009537829925128064	15.2	13.0	5.9	1.0		<-10.28
WD J133013.64−083429.47	3630035787972473600	16.1	12.4	5.6	0.9		
WD J201056.85−301306.63	6749419923164242816	16.2	12.3	5.6	0.9		<-8.84
WD J015202.96+470006.66	356922880493142016	16.5	12.5	5.5	0.9		
WD J211856.26+541241.24	2176116580055936512	17.3	12.4	5.2	0.9		
WD J232847.64+051454.24	2660358032257156736	17.5	13.1	5.0	0.8		-6.58
WD J041630.04−591757.19	4678664766393827328	18.3	12.5	4.9	0.8		
WD J234350.72+323246.73	2871730307948650368	18.6	13.0	4.8	0.8		<-9.53
WD J193713.75+274318.74	2025389380082340992	18.2	13.1	4.8	0.8		
WD J211316.85−814912.88	6348672845649310464	16.2	13.6	4.4	0.7		-8.6
WD J233850.74−074119.97	2439184705619919488	18.6	13.3	4.3	0.7		
WD J162825.00+364615.85	1331106782752978688	15.9	13.8	4.2	0.7	-9.07	
WD J204234.75−200435.94	6857939315643803776	21.8	12.4	4.1	0.7		
WD J202025.46−302714.65	6797171060323993728	17.4	13.6	4.1	0.7		
WD J122642.02−661218.47	5860131207828395648	15.4	13.9	4.1	0.7		
WD J021228.98−080411.00	2486388560866377856	16.7	13.7	4.1	0.7		
WD J212657.66+733844.66	2274076297221555968	22.2	12.9	4.1	0.7		
WD J215225.38+022319.58	2693940725141960192	22.5	12.8	4.0	0.7		
WD J011800.08+161020.56	2591754107321120896	16.8	13.8	4.0	0.7		
WD J112412.97+212135.57	3978879594463300992	14.7	14.1	4.0	0.7		
WD J143307.64−812014.13	5772718006135360128	20.9	13.4	3.7	0.6		
WD J080653.75−661816.70	5274517467840296832	19.2	13.7	3.6	0.6		
WD J015151.14+642552.55	518201792978858880	17.3	13.9	3.6	0.6		<-12.08

Table C1. White dwarfs in the eDR3 catalogue for which a $1 M_J$ planet at 2 au would have a $S/N + \sigma(s/N) > 3$. The data in the first four columns come from [Gentile Fusillo et al. \(2021\)](#). The white dwarf names are WD J + J2000 RA (hh mm ss.ss) + Dec. (dd mm ss.s), equinox and epoch 2000, the distance is the median of the geometric distance posterior (pc) ([Bailer-Jones et al. 2021](#)) and G_{mag} is the corrected photometric G mean magnitude ([Gaia Collaboration et al. 2020](#)). The S/N and error on the S/N were calculated by the authors. The Ca/H and Ca/He data comes from the Montreal White Dwarf Database ([Dufour et al. 2017](#)). This data along with P_{WD} and the white dwarf mass will be made available on Vizier after publication.